MASARYKOVA UNIVERZITA
Přírodovědecká fakulta
Ústav teoretické fyziky a astrofyziky

Diplomová práce

Brno 2019 **Michal Kajan**

MASARYKOVA
UNIVERZITA
PŘÍRODOVĚDECKÁ FAKULTA
ÚSTAV TEORETICKÉ FYZIKY A ASTROFYZIKY

Modelování expandujících obálek supernov

Diplomová práce

Michal Kajan

Vedoucí práce: Mgr. Ing. arch. Petr Kurfürst, Ph.D. **Brno 2019**

Bibliografický záznam

Autor:	Bc. Michal Kajan Přírodovědecká fakulta, Masarykova univerzita Ústav teoretické fyziky a astrofyziky
Název práce:	Modelování expandujících obálek supernov
Studijní program:	Fyzika
Studijní obor:	Teoretická fyzika a astrofyzika
Vedoucí práce:	Mgr. Ing. arch. Petr Kurfürst, Ph.D.
Konzultant:	prof. Mgr. Jiří Krtička, Ph.D.
Akademický rok:	2018/2019
Počet stran:	X + 54
Klíčová slova:	Supernovy; Husté okolohvězdné obálky; Hydrodynamika; Numerické modely; Svetelné křivky

Bibliographic Entry

Author:	Bc. Michal Kajan Faculty of Science, Masaryk University Department of Theoretical Physics and Astrophysics
Title of Thesis:	Modelling of expanding envelopes of supernovae
Degree Programme:	Physics
Field of Study:	Theoretical Physics and Astrophysics
Supervisor:	Mgr. Ing. arch. Petr Kurfürst, Ph.D.
Consultant:	prof. Mgr. Jiří Krtička, Ph.D.
Academic Year:	2018/2019
Number of Pages:	X + 54
Keywords:	Supernovae; Dense circumstellar medium; Hydrodynamics; Numerical models; Light Curves

Abstrakt

V této diplomové práci se věnujeme zkoumání procesů souvisejících s interakcí supernov s hustým rozpínajícím se plynným obalem a jejich následné modelování. Moderní počítače a pokročilé numerické metody jsou schopné řešit složité hydrodynamické rovnice během explozí supernov. V posledních letech se ukazuje, že supernovy nevybuchují v prázdném prostoru, ale v důsledku ztráty hmoty, pravděpodobně kvůli explozivnímu hoření těžších prvků. Interakce supernovy s hustým obalem způsobuje, že tyto supernovy jsou jasnější než běžné supernovy a navíc se tato interakce dá odhalit spektrografií. Využili jsme program na evoluci hvězd pro modelování hvězdy až po okamžik progenitoru supernovy. Následně jsme použili program pro modelování explozí a získaná svetelné křivky jsme porovnali s pozorovanými. Parametry nejlepší exploze jsme porovnali s pracemi jiných autorů.

Abstract

In this thesis, we deal with studies of processes related to supernova interaction with dense expanding gas envelope and their modelling. Modern computers and advanced numerical methods are capable of solving complex hydrodynamic equations during the supernova explosion. However, in recent years it has been shown that supernovae do not explode in the free space, but in the envelope formed of the star's mass loss, probably due to the explosive burning of heavier elements. The supernova interaction with a dense envelope makes these supernovae brighter than conventional supernovae and, moreover, the spectrograph can detect this interaction. We used a stellar evolution program to model a star to get to the moment of a supernova progenitor. Subsequently, we used an explosion modelling program and compared the resulting data with the observed ones. The best explosion parameters were compared with those of other authors.

MASARYKOVA UNIVERZITA
Přírodovědecká fakulta

ZADÁNÍ DIPLOMOVÉ PRÁCE

Akademický rok: 2017/2018

Ústav: Ústav teoretické fyziky a astrofyziky

Student: Bc. Michal Kajan

Program: Fyzika

Obor: Teoretická fyzika a astrofyzika

Směr: Astrofyzika

Ředitel *Ústavu teoretické fyziky a astrofyziky* PřF MU Vám ve smyslu Studijního a zkušebního řádu MU určuje diplomovou práci s názvem:

Název práce: Modelování expandujících obálek supernov

Název práce anglicky: Modelling of expanding envelopes of supernovae

Oficiální zadání:
Výbuchy supernov jsou jedněmi z nejvíce grandiózních událostí ve vesmíru. Poskytují tak neocenitelný pozorovatelský a teoretický materiál pro studium širokého rozsahu fyziky: od kosmologických vztahů k mnohem detailnějším astrofyzikálním procesům, jako je rozsah ztráty hmoty hvězd nebo hydrodynamických pochodů v rámci samotné expanze nebo v interakci s okolním prostředím. Díky prudkému rozvoji počítačů a návazně i numerických metod získala věda velmi mocné nástroje pro podrobné studium a simulace zkoumaných pochodů a jejich následných projevů. Cílem práce je studium procesů, souvisejících s rozpínáním plynných obálek supernov. Půjde o vytváření jednoduchých hydrodynamických modelů, jejich kvantitativní popis i o aplikaci na reálná data. K úspěšnému vytvoření práce je nezbytná znalost příslušných oblastí fyziky, zejména základů hydrodynamiky a teorie hvězdných atmosfér, základů numerické matematiky a běžná rutina v programování. Práce může být napsána česky, slovensky nebo anglicky.

Literatura:
LANDAU, Lev Davidovič a Jevgenij Michajlovič LIFŠIC. *Fluid mechanics*. Translated by J. B. Sykes - W. H. Reid. 2nd ed. Amsterdam: Elsevier, 1987. xiii, 539. ISBN 9780750627672.

BODENHEIMER, Peter. *Numerical methods in astrophysics : an introduction*. New York: Taylor & Francis, 2007. 329 s. ISBN 9780750308830.

PRESS, William H. *Numerical recipes : the art of scientific computing*. Cambridge: Cambridge University Press, 1986. xx, 818. ISBN 0521308119.

ARNETT, David. *Supernovae and nucleosynthesis : an investigation of the history of matter, from the big bang to the present*. Princeton: Princeton University Press, 1996. xviii, 598. ISBN 0691011486.

Jazyk závěrečné práce: angličtina

Vedoucí práce: Mgr. Ing. arch. Petr Kurfürst, Ph.D.

Konzultant: prof. Mgr. Jiří Krtička, Ph.D.

Datum zadání práce: 10. 10. 2017

V Brně dne: 26. 1. 2018

Souhlasím se zadáním (podpis, datum):

.....	.....	.....
Bc. Michal Kajan	Mgr. Ing. arch. Petr Kurfürst, Ph.D.	prof. Rikard von Unge, Ph.D.
student	**vedoucí práce**	**ředitel Ústavu teoretické fyziky a astrofyziky**

Poděkování

Na tomto mieste by som chcel poďakovať v prvom rade svojej manželke Eve, ktorá to som mnou zatiaľ vydržala, rodine, že ma podporovala počas dlhých školských rokoch a strýkovi Petrovi, odpočívaj v pokoji. Chcel by som veľmi poďakovať aj vedúcemu práce, ktorý to so mnou vydržal a naučil ma oveľa viacej ako je v tejto práci.

Prohlášení

Prohlašuji, že jsem svoji diplomovou práci vypracoval samostatne s využitím informačních zdrojů, které jsou v práci citovány.

Brno 16. května 2019 .....

Michal Kajan

Contents

List of Abbreviations

For easier orientation in the text, we presents for the reader an overview of abbreviations that occurs in the whole work.

$M_{\odot}$	Mass of the Sun equals 2×10^{33} g
LC	Light curve
$SLSN(e)$	Super Luminous SuperNova(e)
$SN(e)$	Supernova(e)
$EcSN(e)$	Electron Capture Supernova(e)
ISM	Interstellar medium
CSM	Circumstellar medium
CDS	Cold Dense Shell
WD	White Dwarf
$CCSN(e)$	Core-Collapse Supernova(e)
RSG	Red Supergiant
BSG	Blue Supergiant
LBV	Luminous Blue Variable
WR	Wolf Rayet
NS	Neutron Star
EoS	Equation of the State
Ibc	Ib and Ic
$\log A$	Decadic logarithm or logarithm with base 10 of a number A
BH	Black Hole
kpc	kiloparsecs

Introduction

A supernova explosion is one of the most grandiose events among all that occur in the Universe. Radiation energy, which can be equal to the luminosity of a whole galaxy, is released in the ultimate moment of the ”star's life” [39].

The collapse of the star can happen in a split second.[1] The inner parts of the star are accelerated inwards to a few percents of the speed, and then they instantly stop and bounce, which can lead to an explosion with the similar ejecta velocity speed. The enormous densities and temperatures are reached in the core [24]. Modelling of this event can be complicated because of the extremely abrupt and complex physics of the process connected with the collapsing material bouncing on the proto-neutron star[2] [24] or igniting particular elements[3] [43] that can happen in a very thin layer, while the total mass of the star can also play a significant role.

Nowadays, it is still impossible to solve this problem in general, because of the large amount of data and physical processes that have to be included, so that the model would be physically realistic and accurate. The appropriate physical approximation and modern numerical methods have to be used to solve this problem. The models can be useful even though they are not in perfect agreement with observed data, since they help us to realize whether we did or did not have mistaken during the assumptions as well as it is a perfect way to test new ideas and physics without building expensive physical equipment and infrastructures.

The goal of this thesis is to become familiar with the modelling of supernovae with dense circumstellar medium and obtaining required skills and eventually to assist colleagues with comprehensive exploring of supernovae and their surrounding environments.

[1] In the case of core-collapse supernovae.
[2] In the case of core collapse supernovae.
[3] In the case of type Ia supernovae.

Chapter 1

Theory of Supernovae

1.1 What is a Supernova?

We call a supernova(e) a transient astronomical event(s) associated with the catastrophic explosion of a star in the late stage of its evolution. The name supernova is composed of the Latin word *nova* which means new, and the preposition *super*, added to distinguish them from classical novae, which are by many orders of magnitude less energetic. For a better identification, we label the supernova as SN (see the list of abbreviations), followed by the year of discovery and by letters A - Z in alphabetical order, according to the date of discovery. However, in modern astronomy, we detect many times more SNe than how many letters we have in the alphabet. So, after the letter Z, we start again from aa and create every possible variation. For example, the SN 1999aa was detected as a 27th SN event in the year 1999; we find from the literature sources its discovery on February 11th [52].

What is the exact difference between classical novae and SNe? *First*: the amount of ejected mass in SNe typically exceeds the mass of the Sun, while it is only a fraction of it in classical novae; even if the calculation of the mass of the SN ejecta after the first detection is a non-trivial task. *Second*: it is the difference in luminosity, where the peak for novae is about $4.9 \times 10^{38}\,\mathrm{erg\,s^{-1}}$ [39] while for SNe it varies from $10^{42}\,\mathrm{erg\,s^{-1}}$ to $2 \times 10^{43}\,\mathrm{erg\,s^{-1}}$ [43]. However, there exists the type super luminous SNe (SLSNe), which can be as luminous as $10^{44}\,\mathrm{erg\,s^{-1}}$ [50].

This difference gives the ratio of SNe/novae luminosities of approximately 10^5; we obtain from the Pogson's equation the difference in magnitudes as (easily recognizable) 12.5^{mag}. However, they are even more luminous SN, for example $1.1 \times 10^{52}\,\mathrm{erg}$ of SN 2015L is radiated for 4 months since its detection[13]. However, the luminous energy corresponds to only about 1% of mechanical energy which SNe deliver to the interstellar medium (ISM), and it is only about 0.01% of the energy emitted by neutrinos [39]. This energy distribution was primarily indicated by the detection of neutrinos from SN 1987A.

We have already mentioned that SNe are so luminous that if such events occur in our galaxy and the ISM did not obscure them, they could be comfortably viewed with the naked eye. However, the maximum brightness in the optical range is typically detected in a few weeks after the explosion. Therefore, the observation usually does not provide complete information about the SN early phase. In our Galaxy, SNe were reliably documented at

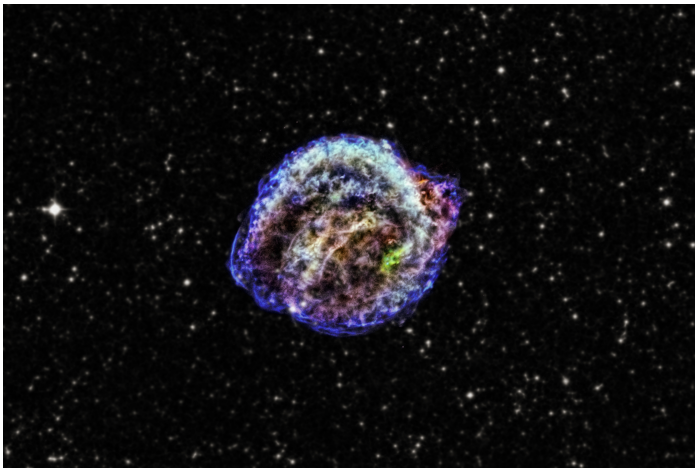

Figure 1.1: Kepler's Supernova remnant in X-rays. Source [26].

least four times in history. The first of them was in the year 1006 in the constellation Lupus with a peak magnitude -7.5^{mag}, and it probably faded away after one year [59]. The next one was discovered in the constellation Taurus in the year 1054 by Chinese astronomers; the remnant of this SN is known as the Crab Nebula. The maximum brightness was probably as high as -6^{mag} [12].

Another one was in the year 1572 in the constellation Cassiopeia. Tycho Brahe did the most precise observations, and in his honor, this supernova is now called Tycho's Supernova (also B Cas). The peak of apparent magnitude was approximately -4^{mag} [2]. Interestingly, it is now considered that this transient object was one of the catalysts for Johannes Kepler, who was not only a contemporary but even the colleague of Brahe, to challenge his world view and ideas about the Universe, which was thought as something unchangeable and unmovable [53]. The next one SN event was observed in the constellation of Ophiuchus, named Kepler's Supernova, in 1604. However, Johannes Kepler likely was not the first one who observed it, but due to his observations made throughout the year, it is called after him. The maximum apparent magnitude of SN 1604 was -2.5^{mag} [57]. Figure 1.1 shows its remnant; this SN type was later classified as type Ia. Each of these SN events appeared as the brightest star in the night sky for some time, before it faded away [56].

Despite the low number of historically observed supernovae, the SN event is not rare, since there occurs approximately one SN event every second within the whole Universe. However, in our galaxy it happens once in 30 - 50 years, but the galactic dust and gas obscure most of them [43]. That is the reason why we do not see them more often. On February 24th, 1987, Ian Shelton and Oscar Duhalde independently observed a SN in constellation Dorado [51]. It was identified that the SN occurs in Large Magellanic cloud, only 50 kiloparsecs (kpc) away, which made it the closest observed SN since the invention of the telescope. Moreover, due to how close it was, we were able not only to identify the progenitor which was a blue supergiant (BSG) star, but we could also see it with the naked eye; 3^{mag} in May, the peak luminosity in visual range reached apparent magnitude 3^{mag} in May. However, it was not the the brightest star in the night sky, because it was not in our galaxy [7]. What was unexpected, was the nature of the SN progenitor. From the theory of stellar evolution it was thought that BSG progenitor could not explode as a

SN while nowadays it is widely agreed that BSGs are possible progenitors for some SN events, if there is involved significant mass loss or high rotation rate [14]. Surprisingly, the neutrino detectors Kamiokande (Japan) and IMB (USA) captured approximately 3 hours before the visual SN appearance twenty neutrinos in the burst that lasted for about 12.5 s. Thanks to this detection, we now better understand the SN physics; this opens new options for research of SNe with the help of neutrino astronomy [39].

We may ask, but why it is crucial to study SNe. This fundamental question has not only one, but many answers and all of them are essential. At *first*, we can say the most important for us is that they produce (either as the progenitor stars during the complete evolution before the explosion or as SNe during the explosion phase) heavier elements than helium (He) and distribute them efficiently to the ISM. This diversity of elements is crucial for us because without it there would be no Earth and no life as we know it. It is estimated that about 10^8 SNe must have exploded in our galaxy up to now, for the metalicity to be so high as we observe. *Secondly*, they inject the kinetic energy $E_{\text{kin}} \approx 10^{51}$ erg into the ISM, which can trigger the collapse of molecular clouds into new stars. *Thirdly*, many years after explosions SNe produce a fraction of highly relativistic particles, so-called cosmic rays, and some specific SNe are probably related to gamma-ray bursts (GRBs). *Fourthly*, due to the observations of the significantly homogeneous type of SNe Ia, we have the evidence that our universe expands and, what is curious, that this expansion accelerates. These facts help cosmology to understand the Universe better [43].

1.2 Classification of Supernovae

If we want to understand something, it is useful first to classify it. The most used classification for SNe was introduced around the year 1934. It is purely phenomenological, and it is based on the spectrum of a supernova at maximum light [56]. Classification process takes place first by looking at the spectra at the peak brightness, to find the presence or absence of Balmer's hydrogen lines. If the hydrogen lines are absent, SNe are classified as type I, otherwise as type II. In consideration of the fact that hydrogen is the most abundant element in the Universe, its absence shows, how specific objects are those of type I. We describe the essential classification process in figure 1.2.

Figure 1.2 shows subtypes of the type I whose classification is based on the presence of silicon lines Si II at 615 nm. To summarize: when H, He, and Si lines absent, we classify the SN event as type Ic, when He lines are present, we classify it as type Ib, and when there are strong Si lines, this SN is of type Ia. However, type II SNe (with H lines) are divided according to either the presence (II-P) or absence (II-L) of a plateau in the LC. A plateau is typically observed after the peak of luminosity and lasts about one month; sometimes it may last for two months or even more [31] [39]. The occurrence of a plateau results from changes in opacity during the recombination process in the expanding and cooling hydrogen envelope [27]. Figure 1.3 shows schematic LCs of SN II-P with plateau phase in contrast to a more classical SN II-L (linear).

We start with type Ia that represents the significant subgroup of SNe: not only do they all have a very similar luminosity and spectral properties, but it also turns out that they are representatives of the specific type of explosion. As we mentioned earlier, the absence of H lines in the type Ia spectra implies some common and special characteristics of their

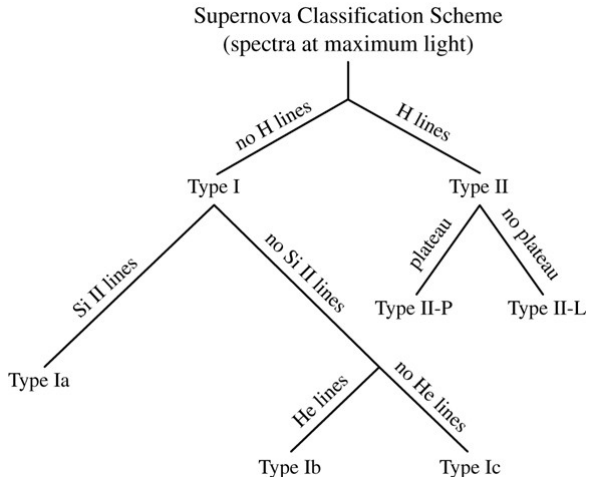

Figure 1.2: The SNe basic classification scheme. Source [39].

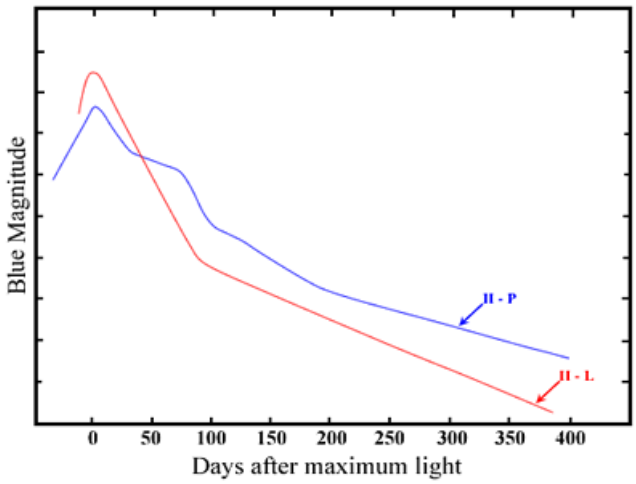

Figure 1.3: Comparison between SN types II-P and II-L. Source [37].

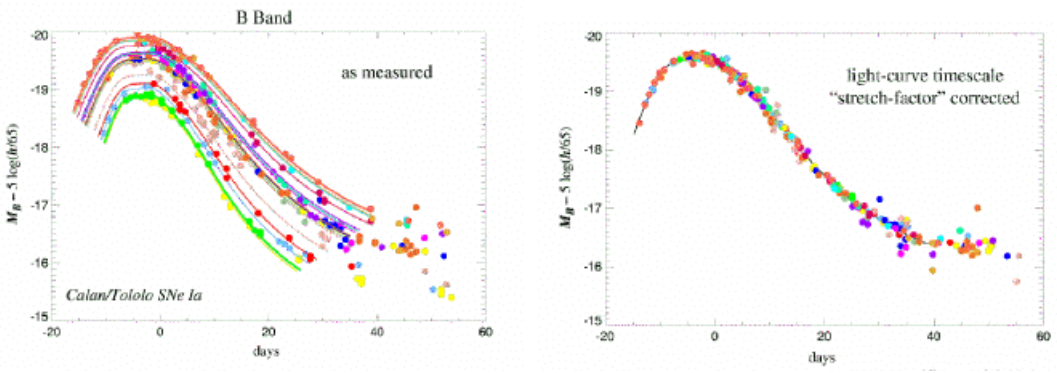

Figure 1.4: Type Ia SNe observed in waveband B. On the left observed LCs on the right LCs after correction (Phillips relation). Source [17].

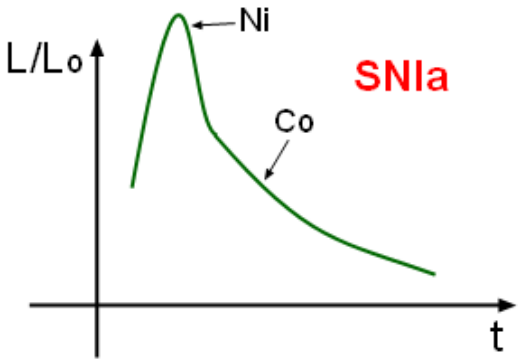

Figure 1.5: LC of SN type Ia with indicated regions of particular radioactive elements decay dominance. Source [48].

progenitors; it is assumed that the progenitor must have been stripped of the hydrogen envelope. The similarity in observables becomes even more evident from figure 1.4; therefore we may use the empirical relation which involves a maximum apparent magnitude and a rate of the stellar magnitude decline near maximum brightness to calculate the maximum absolute magnitude [29]. The equation for calculation of the typical type Ia *intrinsic* (regardless of an interstellar extinction) LC is called the *Phillips relation* (see for example [43], page 121),

$$M_{\max}(\mathrm{B}) = -21.726 + 2.698\,\Delta_{\mathrm{m15}}(\mathrm{B}), \tag{1.1}$$

where $M_{\max}(\mathrm{B})$ is a maximum absolute magnitude in B-waveband, and $\Delta_{\mathrm{m15}}(\mathrm{B})$ is dimming in B-waveband 15 days after peak luminosity. Using Eq. (1.1) and applying the Pogson's equation, we can subsequently calculate from the absolute magnitude the distance of the object [43].

Figure 1.5 shows a schematic LC of SN type Ia. The reason of extended high luminosity after the peak brightness was mystery for a long time. However, it was found out that unstable radioactive ^{56}Ni with halftime decay 6.1 days and then ^{56}Co with halftime decay of 77.1 days are responsible for prolonged luminosity, as is shown in figure 1.5. The high abundance of ^{56}Ni must mean that prior to and during explosion there take place nuclear reactions where C, O, and Si (and other elements) are burned. Figure 1.5 also shows that different decaying elements create different slopes in luminosity. The time-shift between Ni and Co dominated LC is about 50 days which represents a time when a significant amount of ^{56}Ni was decayed [29] [43]. Another characteristic feature is, that the spectrum of type Ia at the maximum luminosity shows not only strong Si II lines but also the lines of O I, Mg II, S II, Ca II, and Fe II [6]. However, there are big differences within type Ia in the amount of produced ^{56}Ni which may range from $0.07\,M_{\odot}$ (SN 1991bg) to $0.92\,M_{\odot}$ (SN 1991T) [43]. One predicts from all of these properties that progenitors of type Ia SNe are WDs in binary systems with various companion star [39]. The remarkable homogeneity of SN Ia enables cosmology to use this type as standard candles to calculate distances. Mainly from observations of type Ia SNe, it was deduced that the Universe is expanding but in an accelerated way. To explain this, cosmologists introduced the so-called *dark energy* whose effects fit the observed data and properties of the Universe /citedarkenergy. It is

estimated that about three-quarters of the Universe consists of the dark energy in current epoch [39].

Next, we continue with SNe types Ib and Ic which have no Balmer H lines, weak or no Si II lines, and the difference between them is only in the presence (Ib) or absence (Ic) of He lines. The absence of these lines in type Ic reveals that no He is present in the progenitor which must have been stripped from H and He stellar envelope. Such stripping could occur either via stellar winds or during a catastrophic nuclear reaction called flash, or in a binary system due to an exchange of mass [27]. The difference between type Ia and both the types Ibc (Ib and Ic) is the absence of Si II lines; this indicates that there is a different physical process responsible for the explosion [39]. Another difference is that the type Ibc SNe are fainter of roughly 1.5^{mag} than the type Ia, but there exist particular cases, when SN can be very bright[1] and can be classified as hypernova[2] or SLSN [31]. Another difference is that the amounts of ^{56}Ni and iron-type elements synthesized in types Ibc are much smaller than in type Ia. Moreover, from the distribution of SNe Ibc, we can deduce that both occur only in spiral galaxies near star-forming regions (near H II regions). This implies that progenitors of both these SN types must be very massive stars. From these facts, we assume that Ibc progenitors are helium cores of massive stars whose H and He envelopes were eventually removed [43].

We close this brief overview with SNe type II, which which are typical for their swift rise in luminosity, while they reach a peak which is little fainter (about 1.5^{mag}) than standard type Ia. However, SNe type II is not a very homogenous class, and they have hydrogen lines where we sometimes observe P Cygni profiles [19]. The primary subdivision of type II into subtypes was described, however, after about 150 days look the LCs similar for any type II SN [43]. When we explore the distribution of SNe type II, they occur only in spiral galaxies, like Ibc. So, the progenitors are also expected to be stars more massive than $8\,M_{\odot}$. After the explosion, we can often find small remnant, NS or BH [43]. For example, SN 1054 was of type II, it is thus not surprising that we could find NS - pulsar in its gaseous remnant, the Crab Nebula [39].

However, it turns out that the more sensitive instruments we use, the smaller details we can observe in each SN event. That makes each new SN event more and more unique and peculiar [43].

1.3 Explosions of the Supernova

SN classification is taxonomic and even since it is useful to divide the observed SNe to more homogeneous subgroups according to similar observables, for example, light curves or spectroscopic properties, such classification criteria have nothing to do with the physical processes of the explosions. Following chapters will describe how stars end as SNe and mechanisms of explosion for different SN classes.

[1] usually at least ten times brighter than standard Ia.

[2] In a hypernova, the velocity of ejecta can reach more than $3 \times 10^4\,\mathrm{km\,s^{-1}}$ [31].

1.3.1 Thermonuclear runaway - Type Ia SNe

Progenitor

The first of all we want to point out that the stellar evolution is not a resolved astrophysical problem. There are many open problems within the stellar evolution theory, for example, winds, convection, or effects of binarity (to name the most important ones). In this chapter, we outline the evolution of the star which is adapted from [21], [27], and [39].

We also describe the basic types of SN progenitors in the next section, where we refer to the stellar structure or composition before and during the process of a SN explosion.

In the beginning, there is a gaseous cloud; if this cloud satisfies Jeans' criterion it starts to collapse.[3] We emphasize that we consider here only the single-stars which is a good approximation for the evolution of stars even in binary systems with sufficient orbital distance between companions. The collapse is halted when gravity force is in equilibrium with pressure gradient which is, however, dependent on the nucleosynthesis stage in a stellar core. Only stars with mass bigger than $0.075 M_{\odot}$[4] reach this equilibrium. The core is heated due to the release of gravitational potential energy by reducing radius; from the Virial theorem, half of the energy stays in the core. At the moment when the gas collapses and thermonuclear reactions ignite, the material of a newly born star is mixed and homogeneous, and primarily made of H and a fraction of He. Thermonuclear burning of H to He in the core takes most of the life of the star; this phase is referred to as the *main sequence* (MS). After this very long phase, H in the core is exhausted, and the equilibrium is disrupted, the star begins to contract. The contraction causes further heating of the central region until H in the shell around the core is ignited. Because the amount of H that burns in the shell is more extensive than it was in the core, the energy production and thus the radius of the star significantly increase. However, as the star's surface expands, the temperature of the surface drops and from Wien's law, the peak of wavelength radiated from the surface shifts to the red; the star moves to the *red giant branch* (RGB).

Explosion

In this paragraph, we describe the explosion of SN type Ia in a way that follows the review in [43]. It is believed to be impossible for WD to explode as SN Ia in case it is originally a single object. However, most stars "live" in binaries or even in multiple systems; and this may lead to SN Ia. There are two alternatives what can be the nature of a secondary star. Moreover, observations indicate that both alternatives occur [58]. The first possibility is that the companion is a non-compact star (MS, RGB, etc.) and the WD accretes the material of its envelope, it is a so-called *single degenerate* model. The WD steadily accretes material until it reaches a critical mass which triggers explosive nucleosynthesis. The second possibility is that a companion is a WD, too, then it is the so-called *double degenerate* model.

In the *single degenerate* scenario, WD accretes H and He envelope of the companion. Simultaneously with the material accretion, H continuously burns on the surface of the

[3] However, many problems are connected with collapse, for example, fragmentation of a gaseous molecular cloud or the angular momentum conservation.

[4] In [27] is the limit little higher than 8% of the solar mass.

WD, producing soft X-rays. The accretion rate cannot be however too fast because of unburnt H can easily ignite uncontrollably; such an explosion may expel more material than was accreted, decreasing the total mass of the WD. These uncontrolled explosions are typical for classical novae. On the other hand, even if the accretion is steady, it takes a very long time for WD to reach the *Chandrasekhar mass* 1.4.4. (noting that average mass of WDs is about $0.6 M_{\odot}$, see the description below in this paragraph). Another weak point of this scenario is that it should be possible to observe at least a little amount of hydrogen, that is provided from the envelope of the companion, in the spectrum.

In the *double degenerate* scenario, both stars evolve more or less simultaneously and so both of them end their lives as WDs. In case the WDs form a tightly bound binary system, we may expect that they emit gravitational waves which is an effective way to lose the angular momentum and get closer to each other. After some time, which depends on their initial orbital distance, they get to the stadium where the WD with lower mass is in the Roche lobe of the more massive one. In this case, the more massive WD successfully disrupts the lighter companion due to tidal forces; simulations show that there forms a thick disk [43]. This scenario explains the absence of H lines in the spectrum; however, the weak point is a very long time from the merger to the explosion, because rapid rotation keeps the structure stable even as the accreting remnant exceeds the Chandrasekhar mass [54]. Another weak point of this model is that due to slow accretion on heavier WD this may collapse into NS by the so-called *accretion induced collapse*; in this case, it does not produce a thermonuclear (type Ia) SN explosion.

Although it is generally agreed that progenitor of a SN Ia is a WD in a binary system, where precisely the ignition starts inside the WD is still an open question. There are two fundamental theories: the first one suggests that the ignition starts at the center of the WD, the second one assumes that the ignition starts off the center (either only slightly off or even near the surface). Another problem, which needs to be resolved to understand the explosions of type Ia better, is the role of the Chandrasekhar mass for WDs to collapse and explode; however, particular distribution of angular momentum by decreasing of effective potential or effects of the magnetic field can alter (increase) the required mass for ignition (super-Chandrasekhar type Ia SN). The traditional and most successful model which explains many SN properties is the model of centrally ignited WD reaching the Chandrasekhar mass; however, recent simulations show that some features cannot be well explained with this traditional model and the new model is needed [30].

We first briefly describe the historical model of the explosion - the *Chandrasekhar mass carbon igniters*. In this model the release of approximately 10^{51} erg of nuclear binding energy can explain observed kinetic energy of the ejecta. This model can also (consistently with observations) explain the abundance of ^{56}Ni, which creates characteristic light curves, and of other elements, too. The most popular is the fact that explosions usually happen near the Chandrasekhar mass, which can explain homogeneity of SNe type Ia. The weak point of this model is the difficulty to explain how to accrete enough mass without undergoing smaller explosions during the accretion process, but at the same time we need enough accreted mass to explain the observed frequency rate of type Ia SNe in the Universe. With more precise and advanced observations we also see that late phases of the LCs are are not in good agreement with this model.

The second significant model of thermonuclear SNe explosions is called the *sub-*

Burning phase	Product (Ashes)	Central temperature in model [$\times 10^7$K]	Timescale
H	He	6	7×10^6 yrs
He	C, O	20	5×10^5 yrs
C	O, Ne, Mg	90	600 yrs
N	O, Mg, Si	170	0.5 yr
O	Si, S	230	6 days
Si	Fe-peak	400	1 day

Figure 1.6: Theoretical results for star with mass $25 M_\odot$. Source [27].

Chandrasekhar mass helium igniters. In this model, He is accreted on the C-O WD, and when He envelope reaches enough mass (around $0.15 M_\odot$), although the total mass is still below the Chandrasekhar limit, the He ignites at the inner edge of the envelope. This advantage of this model is that less material is needed, and so the frequency of SNe is more easily explained.

1.3.2 Core-Collapse

Progenitor

In the previous section 1.3.1 we reviewed the evolution of the star with mass lower than $8 M_\odot$. These stars become WDs via specific mass-loss mechanisms; they usually collapse to WD after getting to AGB phase, and it depends only on the mass of the ZAMS star. However, more massive stars may have different, much more spectacular end. In those stars, temperature and density in the core are sufficient to ignite heavier elements. Burning process scheme in figure 1.6 shows that nucleosynthesis of heavier elements requires higher temperatures, while the timescale for the fuel depletion rapidly decreases [39]. This corresponds to the fact that up to the iron group, the nuclear burning is exothermic; however, the energy excess from nucleosynthesis per nucleus rapidly declines. Together with the increased temperature that accelerates nuclear reactions this all causes that successive phases of nucleosynthesis burn faster. After the iron group is formed, further nucleosynthesis reactions would be endothermic, and there is no possibility to gain any energy from them [27]. Figure 1.7 shows that the iron group nuclei are most strongly bound. We briefly explain why certain chemical elements, for example, He (2p + 2n), O (8p + 8n), Ca (20p + 20n), Ni (28p + 28n), are more stable than the neighboring elements in the table[5] [49]. This is a unique property, and we describe its essential features. Firstly, we imagine that nucleon in the nucleus is in a potential well[6], this concept is similar to the electron shells model. The number of protons and neutrons assembled in the complete shell is called *magic number* (the first few magic numbers are 2, 8, 20, 28). This helps to explain why some elements are more stable than others. However, there is the opposing force - the

[5] Each of these elements is so-called double magic, because there are the magic number for both protons and neutrons.

[6] This concept is also known as the shell model.

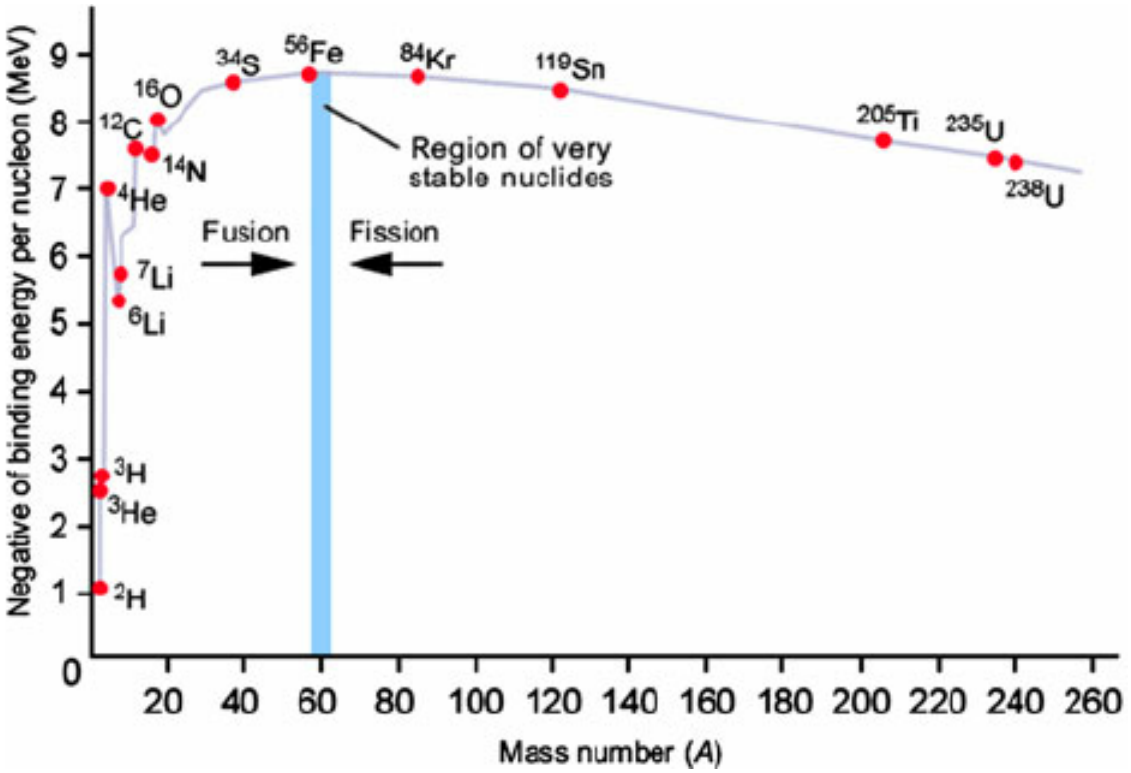

Figure 1.7: Nuclear binding energy. Source [28].

electromagnetic force that affects all the charged particles; because the strong nuclear force is only of the limited range while the electromagnetic force has a wide range, the latter starts to play a more significant role in heavier elements. This is the reason why heavier elements try to compensate this effect with more neutrons in the nucleus (because neutrons are not affected by the electromagnetic force while they effectively contribute to stronger nuclear binding), however, the energy level of neutrons (if we imagine neutrons and protons each separately in a shell, like electrons) cannot be much higher than of protons, because otherwise there develops beta decay [27].

Si burning is the direct predecessor of the end of the star.[7] The structure of the massive stars is like an onion, with heavy elements (the iron group) in the center and successive shells with lighter elements from the previous burning upwards. For the (last) Si nuclear burning the very high temperature (2×10^9 K [29]) is required but at such temperature the neutrino emission begins to dominate over electromagnetic radiation. Even, the neutrino luminosity exceeds several times the electromagnetic luminosity. However, since the neutrino cross-section is extremely small, neutrinos are not being trapped inside the star. This process is very efficient for cooling the over-heated core; because neutrinos easily pass through stellar material, they can easily carry away a significant fraction of produced energy. What is interesting, the specific entropy in the core decreases despite the increase of temperature and density; this can happen due to the electron degeneracy pressure support of stellar core in the late stages of "massive stars' life" [43].

[7] We define the "life" of the star as the period when thermonuclear reactions are the primary source of energy.

Collapse

We sum in this section the main features of the up core-collapse and subsequent explosion of the star as it is described in [24]. The iron core is formed and still grows from ashes of the Si burning. After the mass of the iron core exceeds than Chandrasekhar mass, hydrostatic equilibrium is broken, and the degeneracy electron pressure cannot prevent the collapse of the core. The dominant physical process that contributes to the collapse are: *Firstly*, the temperature, and density high enough to produce neutrino emission. The neutrino emission is an effective tool to remove energy from the core and helps thus to accelerate the collapse. *Secondly*, if the energy of the photons reaches about 1 MeV; they have sufficient energies to disintegrate the nuclei of the iron group. This process is called photodisintegration, and its products are mainly alpha particles and neutrons. *Thirdly*, high energy photons are absorbed by massive particles that are disintegrated to protons and neutrons. The photon energy is absorbed in the process, which enormously accelerates the collapse. *Fourthly*, if the densities increase over $\rho > 10^{11}\,\mathrm{g\,cm^{-3}}$, the Fermi energy of electrons exceeds the energy difference between protons and neutrons, which satisfies conditions for inverse beta decay. This captures free electrons which have so far been the primary source of pressure opposing to gravity and thus helps to collapse [31]. These are the four main reasons why the collapse occurs, and why it is so dynamic.

The gravitational binding energy released during the core collapse is of an order of 10^{53} erg. The energy is converted mostly to neutrinos (about 99%), and the rest is transformed into kinetic energy. From these remaining 10^{51} ergs, only 1% is converted into radiative energy. The speed with which the freely infalling material (in the corresponding gravity field) falls onto the mostly iron core can grow up to an order of $10^{4}\,\mathrm{km\,s^{-1}}$, which can be more than 20% of the speed of light [39]. For illustration, the typical size of the iron core is about the Earth's radius. This leads within the collapsing core to the destruction of all elements produced by nucleosynthesis throughout the whole previous star's life.

Explosion

The collapse of the core is stalled after central density grows to $\rho \approx 10^{14}\,\mathrm{g\,cm^{-3}}$. Then nuclear material bounces in response to the increase of the pressure of the nuclear matter. This creates a massive shock wave that propagates outwards, however, the layers which are outside the homogeneous core continue to infall. If this shock wave is strong enough not only to stop the infall of the outer core but to revert it and to explode the outer envelope, then we call this explosion mechanism as *prompt bounce-shock mechanism*. The energy of the bounce is of the same order as the potential energy released from the core-collapse. However, we know from simulations that the energy of this first shock is mainly absorbed and transferred into dissociation of heavy nuclei within and off the iron core. Simultaneously, a vast number of neutrinos are released, sometimes called neutrino burst at shock breakout. This can lead to slowing down the shock wave and eventually to stalling it; moreover, it can revert the shock wave into accretion shock. Some earlier simulations suggested the prompt shock is the trigger for SN explosion; they are however currently regarded as outdated[8]. After the first shock wave turns to accretion, a compact

[8] Successful prompt explosions were found by simulations only in extremely light stellar iron cores mass of the progenitor $8-10\,M_{\odot}$ or in case of very soft nuclear EoS (see page 41 in [24]).

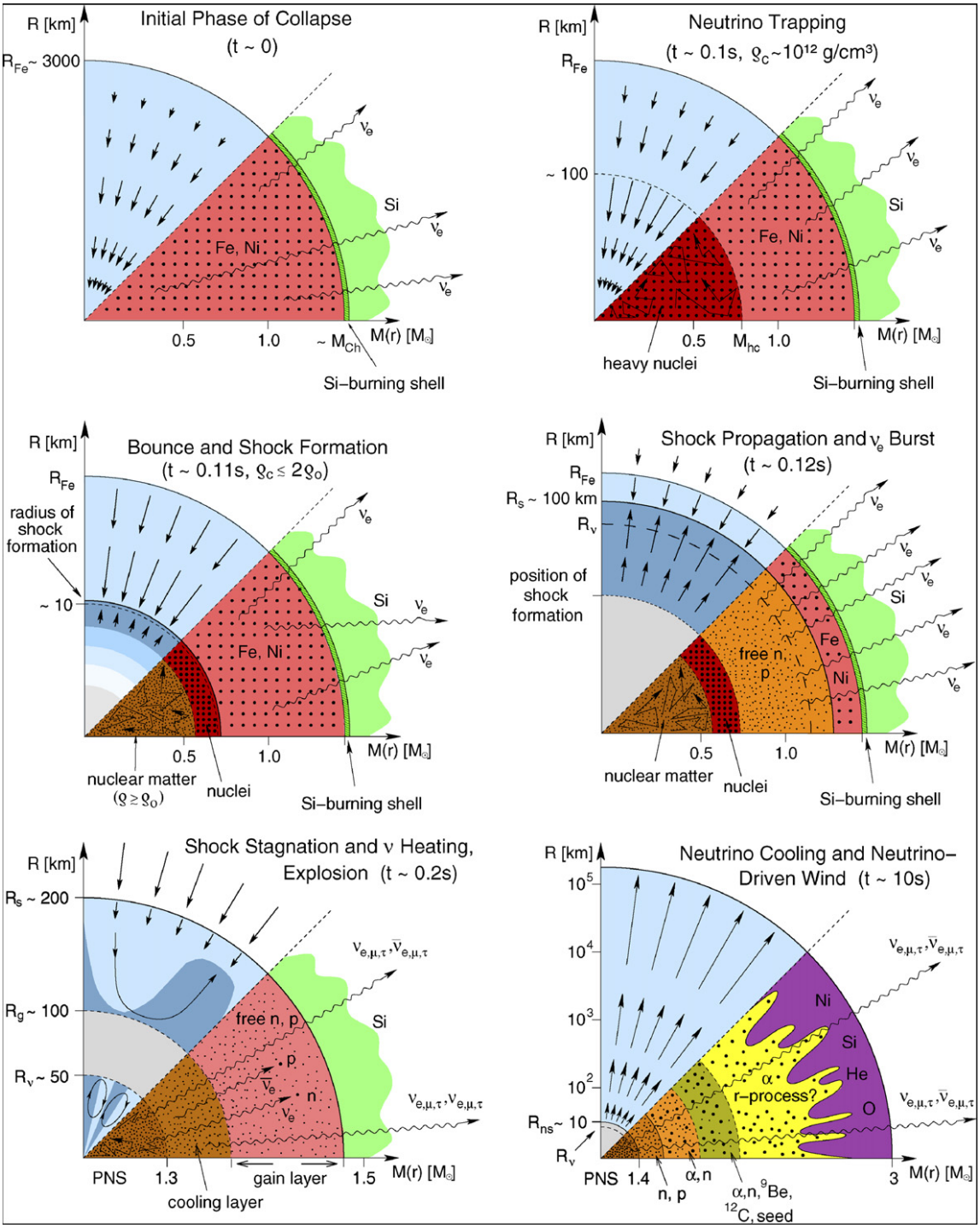

Figure 1.8: Core collapse and SN explosion. Source [24].

object begins to form in the center. Proto-NS rapidly grows due to the accretion of material, and it may evolve to NS or collapse to BH if the progenitor mass was more massive than approximately $25\,M_{\odot}$. Neutrinos from the first infall which were trapped in the proto-NS, diffuse out in few seconds. Consequently, the hot interior of proto-NS is cooled by the production of neutrino-antineutrino pairs [23]. About thirty seconds later a proto-NS

becomes transparent to neutrinos; this effect will decrease the neutrino luminosity.

Another mechanism of the explosion is called *delayed neutrino heating*. In this mechanism, the stalling first shock is revived by neutrinos streaming from proto-NS that are absorbed by the neutrinosphere, which is defined as the layer where the neutrino "optical" depth $\tau_\nu \gtrsim 1$. The certain fraction of the neutrinos (about 1%) is absorbed by this neutrinosphere, which is below the shock and whose energies are converted into the thermal energy of protons and neutrons in the neutrinosphere layer. This layer then starts to expand and creates the region with low density and high temperature behind [24]. However, it seems that also this mechanism is not fully able to explain SN explosions where progenitors are more massive than $11\,M_\odot$. In such more massive stars, the neutrino heating only stops collapse but is unable to drive explosion [31]. The possible efficient mechanism of the explosions can be the *SASI* (standing accretion shock instability). Which can play an important role for asymmetry of SN explosion due to it plays a vital role for neutrinos capturing [20].

1.4 Post supernova evolution

In this section, we make an overview of some processes which are essential for observation of SN. Introducing the *slow* and *rapid* nuclear processes can help us better understand what elements are produced in SNe. Of course, SNe explosions are extremely vital events that provide a plethora of data to study LCs. And, also SN remnants can tell us much about the SNe progenitors.

1.4.1 Abdundances of elements in post-supernova remnant

To explain why we can usually observe in SNe remnants more elements and in a different ratio than it would result from nucleosynthesis theory, we must involve r-process and s-process[9]. Both r- (rapid) and s- (slow) processes are characterized by neutron capture by heavier nuclei and then by the emission of gamma rays, schematically described by the equation

$$n + (Z,A) \leftrightarrow (Z,A+1) + \gamma, \tag{1.2}$$

where Z and A are the proton (atomic) and nucleon (mass) number, respectively. The heavier the nuclei are, the more energy is required for charged particles (for example protons) to overcome the Coulomb potential barrier and to interact with other nuclei. However, this principle does not apply for interacting neutrons, since they have no charge. Neutron interactions are possible even at low temperatures, and the only condition is the sufficient density of neutrons. The resulting nuclei may be stable or unstable to beta-decay [31].

There is a struggle between neutron capture and beta decay; if the timescale for beta decay is lower than the timescale for neutron capture, there occurs the s-process, where the nuclei have enough time after the neutron capture to undergo beta decay. This reaction

[9] For some proton-rich isotopes it is necessary to include also the p-process which occurs if proton flux is high enough; however, the abundance yields from the p-process are even in maximum about two orders of magnitude lower than from r-and s-process for a given element.

produces directly (beta decay is not involved) or indirectly (through the beta decay) very stable nuclei. However, if the timescale for beta decay is higher than for the neutron capture, (the reason can be for example the vast number of neutrons around, produced due to the transition of the shock wave), then starts the r-process. Within the r-process, a beta decay cannot occur, however, there can be multiple neutrons captures, and the products are typically neutron-rich nuclei [39]. The s-process may occur at various stages of stellar evolution (for example in AGB stars) because many reactions can produce free neutrons. Also, these free neutrons in stellar plasma have enough time to interact with nuclei and create (generally called) s-isotopes. In order for the r-process to occur, a massive flow of neutrons is required, which usually occurs only in the late stages of stellar evolution (or after the first bounce of the collapse near the core). Although some isotopes can be created by s- or r-process, the way it happened cannot be determined reversely for a given nucleus.

As the shock wave from SN explosion propagates through the onion-like structure of the star, there takes place, especially the r-process. However, both the processes contribute to abundances of nuclei with $Z > 60$ [27] .

1.4.2 Supernova Remnant

After the SN event, the ejecta continue to travel through the surroundings and transfer a a substantial amount of energy to ISM and sweep the surrounding material. This problem is thoroughly described in [46]; we reproduce here only the first part of these assumptions. The reason for that is that only the first phase (in the first years) affects the LC, as we will see. To describe the whole process exhaustively would be complicated; however, we can divide it into different phases, according to dominant physical processes. The same division, following the same assumptions, is used, e.g., in [43]. We will fully describe here only the first phase where we attach the analytical relations for the typical expansion velocities, time-scales, and length-scales. For the following later phases, we only briefly mention some of their properties.

In the *initial phase* after the explosion, ejecta travel through ISM with a constant supersonic speed. This may happen because the density of the ISM is very low and has very little influence on the expansion of the shock wave. To calculate the average expansion velocity, we need to know only the energy of explosion and mass of the ejecta,

$$E_{\mathrm{SN}} = \frac{1}{2} M_{\mathrm{ej}} \langle v_{\mathrm{ej}}^2 \rangle \implies \langle v_{\mathrm{ej}} \rangle = \left(\frac{2E_{\mathrm{SN}}}{M_{\mathrm{ej}}} \right)^{1/2}, \tag{1.3}$$

where E_{SN} is SN energy, M_{ej} is mass of the ejecta, and v_{ej} is velocity of the ejecta. The distance at a maximum speed is

$$R_{\mathrm{ej}} = v_{\mathrm{max}} t, \tag{1.4}$$

where, if t is the time since explosion, so R_{ej} is radius of the expansion front; v_{max} may be typically $\sqrt{5/3}\langle v_{\mathrm{ej}} \rangle$ in case of a constant or sufficiently flat density of the ejecta. As the shock wave moves through ISM, it gradually accumulates its mass. The end of the first phase corresponds to time, when the mass accumulated during this first phase equals the initially ejected mass,

$$M_{\mathrm{ej}} \sim \frac{4\pi}{3} R_{\mathrm{sw}}^3 \rho_{\mathrm{ISM}} \implies R_{\mathrm{sw}} \sim \left(\frac{3M_{\mathrm{ej}}}{4\pi\rho_{\mathrm{ISM}}} \right)^{1/3}, \tag{1.5}$$

where R_{sw} is the so-called sweep-up radius and ρ_{ISM} is the density of ISM, we can assume it as constant. We calculate the time-scale of the first phase ,

$$t_{\mathrm{sw}} = \frac{R_{\mathrm{ej}}}{v_{\mathrm{max}}} \implies t_{\mathrm{sw}} \sim \frac{\left(\frac{3M_{\mathrm{ej}}}{4\pi\rho_{\mathrm{ISM}}}\right)^{1/3}}{\left(\frac{2E_{\mathrm{SN}}}{M_{\mathrm{ej}}}\right)^{1/2}}, \tag{1.6}$$

which for some typical values in SN, that is, $E_{SN} = 10^{51}\,\mathrm{erg}$, $M_{\mathrm{ej}} = 1\mathrm{M}_{\odot}$ and $\rho_{\mathrm{ISM}} = 2\times10^{-24}\,\mathrm{g\,cm^{-3}}$ [46], gives $t_{\mathrm{sw}} \approx 6,3\times10^{9}\,\mathrm{s} \approx 200\,\mathrm{yrs}$. Near this sweep-up time the SN remnant structure changes, it is due to the reverse shock begins to travel inwards (considering the laboratory frame); this creates a flat profile structure of supernova remnants and the reverse shock-heats the inner layers to higher temperatures [46].

In the following *adiabatic* phase we can assume that radiation processes are negligible, which means that energy during this phase is constant. Because the SN remnant has nearly flat pressure profile and is very hot, the following expansion can be considered as adiabatic. G. I. Taylor and L. I. Sedov analytically derived the solution for such a pressure-driven explosion (see pages 230 - 240 in [46]). This is the reason why we sometimes call this phase the Sedov phase. As time increases, the velocity of the shock decelerates together with decreasing temperature. After the temperature drops down to millions of Kelvins, ionized atoms start to capture free electrons and emit radiation, which affects (decreases) kinetic energy; this is the ultimate condition for this phase.

In the successive *radiative* phase, radiative losses become dominant, and the expansion of dense outer shell is mainly driven by the hot internal layers. The shell expands with constant momentum and begins to accumulate ISM as a snowplow; this is why this phase is referred to as the snowplow phase. As the velocity further decreases, the outer shell breaks up into clumps and they start to merge with the surrounding ISM. This happens after the expansion velocity drops to typical values of the thermal velocity of the ISM [43].

1.4.3 The collapsed remnant of the supernova core

1.4.4 White dwarf

As soon as WD is formed, it starts to cool down. The cooling down does not affect the EoS, because the star is supported with *electron degeneracy pressure*, which does not depend on temperature. The electrons that are freely moving in the gas produce the electron degeneracy pressure due to the *Pauli exclusion principle* that states that two fermions (with the same spin) cannot simultaneously occupy the same quantum state. This adds to electrons a significant amount of (non-thermally provoked) momentum. However, massive particles cannot reach the speed of light, anyway, after some electrons reach relativistic speeds, the electron degeneracy EoS softens. The result of the existence of the particular limit in mass $M \approx 1.44\,M_{\odot}$ (called Chandrasekhar mass, see also section 1.3.1), over which the WD collapses to NS[10]. However, the characteristic property of the degenerate material

[10] This mass can be higher if the WD spins fast.

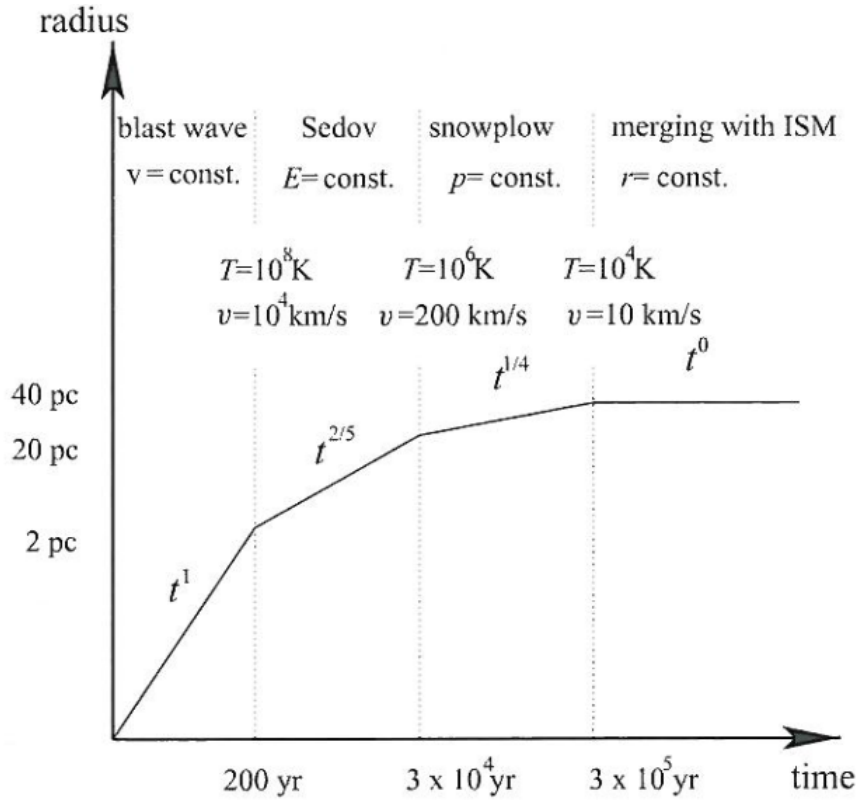

Figure 1.9: Four phases of SN remnant evolution. Source [43].

of WDs is that the total mass is inversely proportional to the radius; this results from the already mentioned EoS of the electron degenerate gas.

We know from observation that the distribution of WDs' masses ranges from $0.2\,M_\odot$ to the Chandrasekhar mass, the statistical peak is around $0.6\,M_\odot$. The chemical composition of the typical WD depends on its mass, those that are lighter than about $0.45\,M_\odot$ are mainly made from He, while the heavier mainly consist of C and O. We again note the important thing that WDs are expected to be (under the particular conditions) the progenitors in SNe type Ia [43].

1.4.5 Neutron star

NS is a product of CC SNe, and it is, in fact, the degenerate core of its progenitor. From the physical point of view, the NS can be viewed as one large nucleus held together by gravity and supported by neutron degeneracy pressure. The mass of NS must be higher than the Chandrasekhar mass (see section 1.4.4). However, their maximum mass is limited, too. If the mass exceeds approximately $3\,M_\odot$, the neutron degeneracy pressure cannot support the mass against gravity and the star collapses to a singularity. For example, radius of the typical NS is about 20 km and the density in the center can reach $\rho_c = 10^{15}\,\mathrm{g\,cm^{-3}}$ for $M_{\mathrm{NS}} = 1.4\,M_\odot$ [39]. Under such densities (as are present in the center) are the properties of the matter very poorly understood. The exact solution of the neutron degeneracy EoS is only assumed, which causes uncertainties about the maximum mass of NS. It was both

theoretically explained and observationally confirmed that to satisfy the law of angular momentum conservation, NS stars must spin extremely fast, even if the degenerate core initially rotated only slowly (pulsars may have rotation periods in milliseconds). From the same argument, their magnetic field is enormous (10^{10} Tesla [27]), too. Pulsar is isolated, rotating NS with a powerful magnetic field. Because only the neutron degeneracy pressure plays a role in the EoS, they must obey principles similarly as white dwarfs, namely that they shrink in size and thus become more dense with increasing mass [39].

Chapter 2

The Supernova interaction with circumstellar media

2.1 Supernova type IIn - interacting with the CSM

Supernova type IIn was separated from type II in 1990 when some supernovae start to show a narrow profile in hydrogen instead of P Cygni profile [45]. The narrow line of H is superimposed on the more broad H line. First of all, type IIn is not caused by a different type of explosion or progenitor, but supernova with dense envelope around. For example, a supernova can be identified as type Ia, then change to IIn, thanks to some hydrogen-rich circumstellar media not necessary near around the progenitor, for example, SN 2002ic.[3] Interaction of SN ejecta with the dense circumstellar medium can tell us lots about last months, years or even centuries of the star and can help us to better understand explosive burning of elements or the physics of formation very strong winds.

2.1.1 Work by Nathan Smith.

In this section, we summarize work by Nathan Smith [47].

Supernova type IIn is classified as SN with narrow Balmer H lines in the spectrum. The narrow lines are not unique for type II, as they were observed more than ten years ago in SN type Ib with narrow He lines. SN Type Ib with narrow lines created subtype Ibn, with the prototype is SN 2006jc.

SN IIn does not need an explanation as a new type of explosion, as they are CC SNe identical to Ib, Ic or II; however, it is considered that around SN is an external factor. Therefore there does not exist an evolutionary path for the star to explode as SN IIn, neither there is no specific progenitor for which is this included. However, the main difference between classical SN and SN IIn is that they convert a portion of kinetic energy to luminosity. This transformation of energy occurs in the collision of the supernova ejecta and circumstellar medium (CSM). The efficiency of this transformation can be different, considering the parameters as the speed of ejecta or density profile of CSM. It is interesting, that this diversity, for example, provides problem to point out progenitor because WDs with very dense CSM can look similar to very massive luminous blue variable stars (LBV).

To sum up, the SN IIn is any SN which originally resided within sufficiently dense or

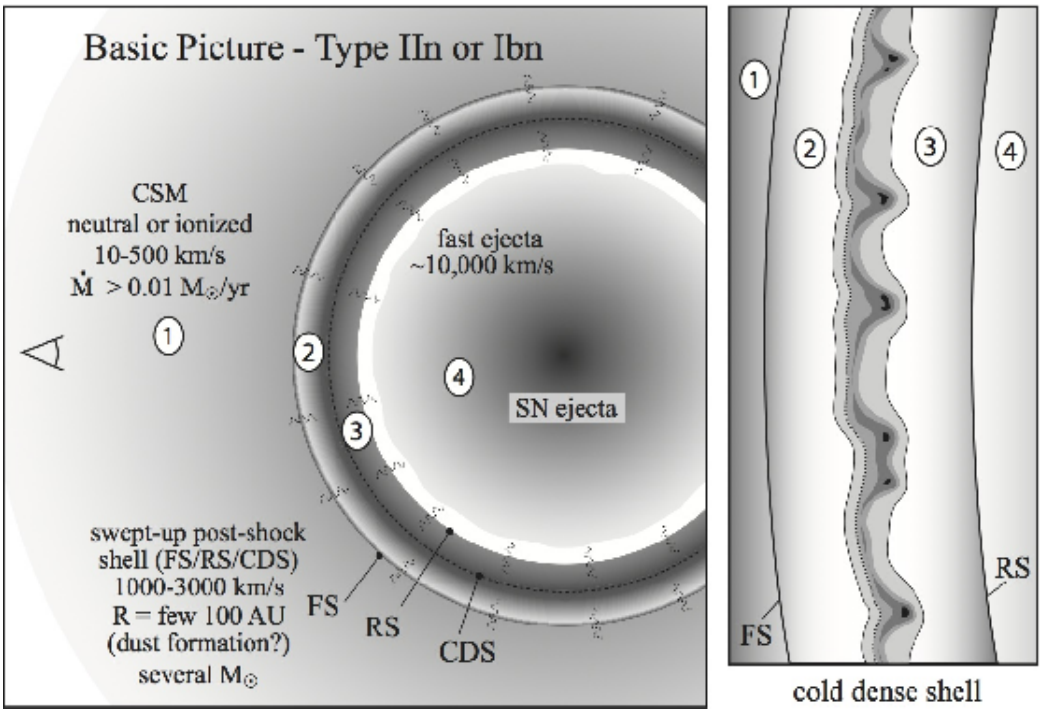

Figure 2.1: Sketch of basic picture with of SN interacting CSM. On the right panel is magnified dividing line between zone 2 and 3. Source [47].

huge H envelope. Moreover, all SNe interact with some envelope as space is not completely empty.

Mechanism

We can divide the region where SN IIn occurs into four zones. The first zone is a location where CSM is unshocked outside the forward shock; this zone is photoionized. The second zone is the location where CSM is hit by the forward shock, but not by the SN ejecta. The third zone is a location where SN ejecta meets reverse shock and is decelerated. The fourth zone is freely expanding SN ejecta. In classic supernova[1] we can observe only the fourth zone. However, in classical SN IIn all four zones can contribute at the same time to the observation. At the early time of SN, the photosphere[2]) is in zone 4 (noted in the unshocked CSM), so that the inside shock wave is obscured, which leads to the ionization of CSM. The emission comes mainly from electron scattering, which prevents us to see the shock wave inside. At this time, the spectrum usually looks like a blue continuum with narrow emission lines that contain broad Lorentzian wings. The shock wave propagates. However, it is an interesting fact that the wings are not caused by the shock wave, but by electrons in the dense unshocked CSM which interact with photons. When the photosphere moves deeper to zone 2 and 3, we can see changes in the spectrum when observing the shock wave. This phase occurs during the luminosity peak, which allows us to see lines with

[1] Without CSM.

[2] Location where $\tau = 2/3$, τ is optical depth, the surface where the nearly all photons are emitted without absorbed by the successive envelope, excluding interstellar dust. Definition from [39]

intermediate width (that is equal to the speed of a few $10^3\,\mathrm{km\,s^{-1}}$) and sometimes with the P Cygni absorption profile. Moreover, the radiation from post-shock gas is observed. By definition, the very hot gas is rapidly radiatively cooled, which means that the zones 2 and 3 sometimes merge into one very thin layer. It is expected that this cooled gas is very dense due to the CSM accumulation onto the ejecta; this layer is then referred to as a *cold dense shell* (CDS). If we look at the SN IIn in the spectrum, we would see strong H (IIn) or He lines (Ibn). The CDS can contribute to the spectra even after photosphere recedes. After the luminosity peak, the photosphere recedes deeper into the freely moving SN ejecta which is marked as zone 4 in the figure 2.1. It is important to realize that starting observation at this time would lead to not being able to notice the strange phenomenon of SN interacting with the CSM. Due to this fact, the observer would only see P Cygni profile from the freely moving SN ejecta or the radioactive powered SN remnant. The duration and strength of the interaction between the CSM and SN ejecta are heavily dependant on the duration and velocity of the pre-mass loss of given SN, not on the explosion. This was only a basic overview, on the other hand, the real situation may be hugely complicated. The CSM can be disky, onion-like structured or purely asymmetric (from explosive mass loss), which would cause that the lines would not be seen, or in a different case, the photosphere would be on all four zones at the same time, which would create unique spectra. Additionally, the total luminosity produced by interaction with the CSM can be relatively high. Without considering efficiency conversion of kinetic energy to luminosity that can be up to 50% (in classical SN only up to 1%), it would not be possible to explain the super-luminous SN (SLSN) type IIn with typical energies of the explosion.

We will mention below one more realistic case, which would create an SN without any trace of type IIn. When the CSM forms a disk, the SN ejecta and photosphere engulf the disk. Narrow lines are formed in the CSM, ionized by highly energetic photons generated during the shock breakout, but in this case, we would not see photons from the CSM, because they would be absorbed and reradiated by SN ejecta. The only hint would be when the fraction of kinetic energy of ejecta hits the disk which leads to its heating. The hot disk would radiate energy which heats remaining SN ejecta, therefore the resultant SN would be more luminous than typical type IIP. This example may be applied to many SN II.

The main free parameters which characterize the supernova are the mass of the ejecta, kinetic energy, including radioactive decay, and the composition and structure of the progenitor. However, in the interacting supernova, we must also include the CSM mass, the density distribution of the CSM as well as the geometry. Besides, while it is possible for us to divide the SN into different classes, the interactions with the CSM show that the SN type can be changed from time to time.

Observed subtypes

Further on in this chapter, we will describe some emerging trends[3] about the behaviour of SN IIn.

Enduring IIn (examples: SN 1988Z, SN 2005ip). They have smooth blue continuum and intermediate width of hydrogen lines. Some cases show strong coronal emission line

[3] In work [47] there classified more emerging trends; however, we choose for this overview only those which apply to our thesis.

implying the photoionization of the Dense CSM by X-Ray generated from the shock. They are more luminous than typical IIP but not as much as SLSN. They fade very slowly and sometimes show signs from the CSM interaction over the years. While SLSN has high CSM mass (probably created by LBV or RSG explosive burning) enduring IIn needs lower mass which can be explained by the relatively stronger red supergiant wind for years. They are *standart* representatives of type IIn.

Transitional IIn (examples: SN 1998S, PTF11iqb, SN 2013cu). This class shows the signature of a very brief interaction with CSM (usually for the first few days) and can be missed if we do not observe it immediately after the explosion. It is indicated that the mass of the CSM is of an order $0.1\,M_{\odot}$. Then this class metamorphs into II-L or IIb. However, it is interesting that at later times the CSM interaction can be detected again. For this class it is unknown how often it occurs.[4]

Type IIn-P (examples: SN 1999W, SN 2011ht). This is a subclass of IIn, which exhibit IIn spectra, but have LCs with clear plateau drop. But not confused them with type IIn/II-P, which have narrow lines at early times and then evolve into "normal" SN II-P. In type IIn-P the strong P Cygni profile is visible in the narrow H lines during their bright phase. After the bright phase, drop from the plateau phase is very intense(several magnitudes). They may be caused by EcSN with low energy of explosion $\approx 10^{50}$ erg.

SN IIn Impostors (example: LBVs, SN 2008S). Sometimes the transient object can look like SN IIn. It has also narrow hydrogen lines, but it is fainter (absolute magnitude in R band is around $M_{\mathrm{R}} \simeq -15.5^{\mathrm{mag}}$), as well as it obtains slower velocities than SN IIn. This may be caused by the non-terminal eruption of LBVs. Declaring that all impostors are not SNe, would lead to the removal of the real "failed" SNe. "Failed" SNe are caused by the fallback to a black hole or pair-instability SNe or even SN from BSG with a low mass of the nickel in the ejecta.

The velocity of the wind is generally proportional to the star's escape velocity; however, this is true only for radiation-driven winds. The CSM velocity does not obey this condition for wind, the CSM may cause explosive burning or explosions which can explain lower velocities, or it may be accelerated with radiation which in turn causes CSM velocity to be higher.

2.1.2 Work by Takashi Moriya.

In this subsection, we make an overview of the significant and important work by Takashi Moriya from [33]. SNe IIn have narrow core hydrogen lines in spectra. It is assumed that this component is formed in dense CSM which surrounds progenitor. As the shock passes through CSM the kinetic energy is converted to thermal energy; however, thermal energy is very efficiently cooled by radiation which makes this transient object very bright. In summary, the kinetic energy is converted to radiation in timescale (years or decades) due to the interaction with dense CSM, instead of slowly fading as typical supernova remnants with timescale $\approx 10^6$ years.

The mass-loss rates in type IIn are estimated range from $\sim 10^{-4}\ M_{\odot}\,\mathrm{yr}^{-1}$ to $\sim 10^{-2}\ M_{\odot}\,\mathrm{yr}^{-1}$, however this is much higher than mass-loss from typical SN progenitors.

[4] There is a problem with undetectable luminosity in late stages.

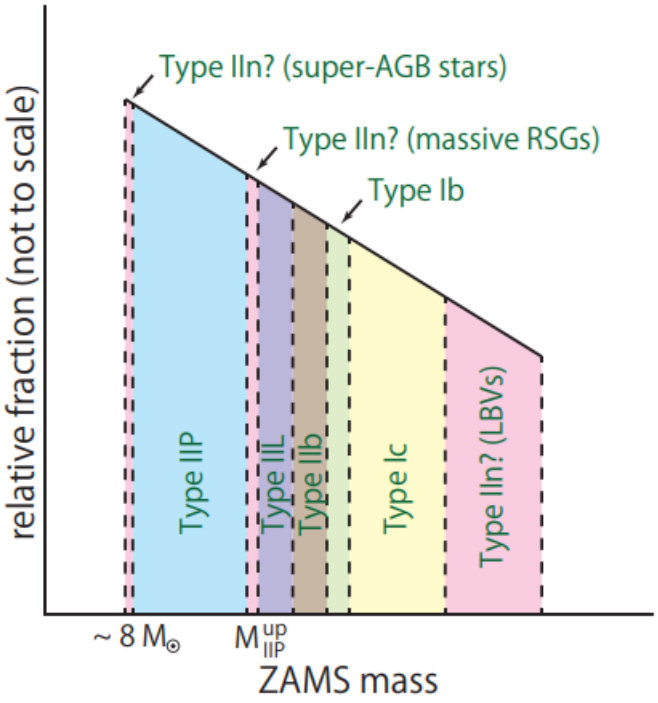

Figure 2.2: Possible connection between ZAMS and SN explosion type. Source [33].

The typical progenitors have mass loss rates $\leq 10^{-5}\, M_{\odot}\,\mathrm{yr}^{-1}$. However, some possible SN progenitors can experience enhanced mass loss before their explosion.

The first type of SN progenitor with enhanced mass loss is electron capture SN (EcSN) in the mass range $8-10\,M_{\odot}$, where CSM is formed during star's super-asymptotic giant branch period. The study that compares the location of SN and Hα emitting regions in galaxy shows that SNe IIn are preferably of relatively low mass progenitors ($8-10\,M_{\odot}$).

The second possible progenitors can be of a mass range between a mass of maximal SN II-P and minimal SN II-L progenitors. However, there are many discrepancies between the determination of this value. From the observations it is stated $17\,M_{\odot}$, but from simulations this value is even $25\,M_{\odot}$. Progenitors of II-P are RSGs but it was revealed recently that high mass loss from massive RSG is consistent with the fact that massive RSGs are theoretically unstable. Their radius is so large that temperature is low and kappa-mechanism (enhanced wind mass loss rate due to higher opacity in lines at lower temperature) or g-mode oscillation [5] of the core can enhance RSG mass-loss before their explosion. However, if massive RSG exists then it would explode as type IIn.

Third possible type of for IIn is a very massive star which becomes LBV during the last stage of evolution. It is known that LBV has a very extensive mass loss. The most known and famous example is η Carinae with a mass roughly $120\,M_{\odot}$ and mass of the CSM around $10\,M_{\odot}$.

This three types can probably explain the heterogeneity of SN IIn, from underluminous

[5] G-mode oscillation of the Sun are "oscillations of the solar interior for which buoyancy acts as the restoring force" [1]

SN (EcSN with low Ni mass) to very bright SLSN (progenitor is LBV star).

2.2 Supernova interaction with thin CSM

2.2.1 Basic hydrodynamics

In this subsection we will prepare a specific equation which we used in deriving later. Spherical continuity equation is

$$\frac{\partial \rho}{\partial t} + \frac{1}{r^2}\frac{\partial}{\partial r}\left(r^2 \rho v_r\right) = 0. \tag{2.1}$$

If we assume density with a power law as

$$\rho = A r^n t^s. \tag{2.2}$$

Then, after using a basic adjustment we get

$$A t^{s-1} r^n (s+n+3) = 0. \tag{2.3}$$

For for eq. 2.4 to hold, the brackets must equals to zero, and the ρ is then

$$\rho = A r^n t^{-n-3} = A t^{-3}\left(\frac{r}{t}\right) = t^{-3} f(\mathrm{v}), \tag{2.4}$$

where we define f(v) as arbitrary function of r/t.

The Rankine-Hugoniot conditions are for describing the relationship between two states divided by shock wave. While they hold for coordinate frame co-moving with discontinuity. We write here the second condition for the conservation of momentum in 1D. Then we arrange it to have pressure on one side.

$$\rho_1 u_1^2 + p_1 = \rho_2 u_2^2 + p_2 \tag{2.5}$$

$$[\rho_1 u_1^2 - \rho_2 u_2^2] = p_2 - p_1 \tag{2.6}$$

$$[\rho_1 u_1^2 - \rho_2 u_2^2] = \Delta p = \frac{F}{S} = \frac{Ma}{S} \tag{2.7}$$

$$S_{sh}[\rho_1 u_1^2 - \rho_2 u_2^2] = M_{sh}\frac{dv_{sh}}{dt} \tag{2.8}$$

2.2.2 Analytic solution of expanding shocked dense shell

In this section, we describe an analytic formalism of the interaction of shocked dense shell inside of circumstellar media. It would be based on certain simplifications and assumptions; however, similar assumption and principles were used in many works, e.g., [9] [10] [33].

We would assume that after the shock wave passes through the surface of the star, which is in case of a thin CSM at the same time a shock breakout, the ejecta continue following the homologous expansion with velocity

$$v = \frac{r}{t}\,\rho = t^{-3} f(\mathrm{v}). \tag{2.9}$$

If we substitute this Eq. 2.1, we get equation 2.4. Next, the shocked dense CSM and SN ejecta create thin dense shell due to the effective radiative cooling. We assume that the thickness of the dense shocked shell is much smaller than its radius, and we denote the radius of the dense shocked shell (time-dependent) $r_{\mathrm{sh}}(t)$. Moreover, if we want to describe the density profile in the progenitor more realistically, we must use at least two power laws to joins the changing profile of density. First power law for inner parts (the core), and the second one for outer parts (envelope). The density will be then proportional to the radius on the power of δ and n for inner and outer parts, respectively.

$$\rho_{\mathrm{in}} \propto r^{-\delta},\ \rho_{\mathrm{ej}} \propto r^{-n} \tag{2.10}$$

In the last ρ_{in} is a density of the inner part and ρ_{ej} is a density of the outer part. The typical values are $n = 12$ and $\delta = 0-1$ for RSG [38]. We scale the equations for densities with multipliers B_{in} and B_{out} for inner and outer parts of the star, respectively. Then we substitute these equations again to the spherical continuity equation 2.1, we get

$$\rho_{\mathrm{in}} = B_{\mathrm{in}} t^{-3} v_{\mathrm{tr}}^{-\delta} = B_{\mathrm{in}} r^{-\delta} t^{-\delta-3} \quad (r < r_{\mathrm{tr}}), \tag{2.11}$$

$$\rho_{\mathrm{out}} = B_{\mathrm{out}} t^{-3} v_{\mathrm{tr}}^{-n} = B_{\mathrm{out}} r^{-n} t^{-n-3} \quad (r > r_{\mathrm{tr}}), \tag{2.12}$$

where the subscript $_{\mathrm{tr}}$ denotes the transition region, these equations apply if the shock wave is in this region. But from homologous expansion we can transform radius to velocity, because at radius r_{tr} a shock wave has velocity v_{tr}. We need further to express total mass and energy. However, we must integrate both mass and energy separately in the inner region and outer region (noting region is defined as a place with different slopes of density). We use simple limits in integral that $0 < r_{\mathrm{in}} < r_{\mathrm{tr}}$, $r_{\mathrm{tr}} < r_{\mathrm{sn}} < \infty$. Equation of mass integration are

$$M = 4\pi \int \rho r^2 dr,$$

$$M_{\mathrm{in}} = 4\pi B_{\mathrm{in}} t^{\delta-3} \int_0^{r_{\mathrm{tr}}} r^{2-\delta} dr = \frac{4\pi B_{\mathrm{in}} v_{\mathrm{tr}}^{3-\delta}}{3-\delta}, \tag{2.13}$$

$$M_{\mathrm{out}} = 4\pi B_{\mathrm{out}} t^{n-3} \int_{r_{\mathrm{tr}}}^{\infty} r^{2-n} dr = \frac{4\pi B_{\mathrm{out}} v_{\mathrm{tr}}^{3-n}}{n-3}, \tag{2.14}$$

while the equations for energy intergration are

$$E = \frac{1}{2} \int \rho v^2 dV,$$

$$E_{\text{in}} = 4\pi B_{\text{in}} t^{\delta-5} \int_0^{r_{\text{tr}}} r^{4-\delta} = \frac{4\pi B_{\text{in}} v_{\text{tr}}^{5-\delta}}{5-\delta}, \tag{2.15}$$

$$E_{\text{out}} = 4\pi B_{\text{in}} t^{n-5} \int_{r_{\text{tr}}}^{\infty} r^{4-n} = \frac{4\pi B_{\text{out}} v_{\text{tr}}^{5-n}}{n-5}. \tag{2.16}$$

The difference between inner and outer part for both energy and mass is that denominator elements are swapped (different limits of the integral). We know that density in the expanding envelope changes continuously, which is reflected by the following boundary condition:

$$\rho_{\text{in}}|_{r_{\text{tr}}} = \rho_{\text{out}}|_{r_{\text{tr}}}. \tag{2.17}$$

If we substitute densities from equations 2.11 and 2.12, we get

$$B_{\text{in}} r_{\text{tr}}^{-\delta} t^{-\delta-3} = B_{\text{out}} t^{-n} t^{-n-3},$$

$$B_{\text{out}} = B_{\text{in}} v_{\text{tr}}^{n-\delta}. \tag{2.18}$$

Equation 2.18 shows dependence between coefficients. If we want to express velocity as kinetic energy with mass and energy, at first we need express density coefficient using the mass, so we express the equations 2.13 - 2.16 using the mass and the energy of the ejecta.

$$M_{\text{ej}} = M_{\text{in}} + M_{\text{out}} = \frac{4\pi B_{\text{in}} v_{\text{tr}}^{3-\delta}}{3-\delta} + \frac{4\pi B_{\text{out}} v_{\text{tr}}^{3-n}}{n-3}. \tag{2.19}$$

Using the equation 2.18, we get

$$M_{\text{ej}} = \frac{4\pi B_{\text{in}} v_{\text{tr}}^{3-\delta}(n-\delta)}{(3-\delta)(n-3)}. \tag{2.20}$$

The inner coeficient of the density then is:

$$B_{\text{in}} = \frac{M_{\text{ej}}(3-\delta)(n-3)}{4\pi v_{\text{tr}}^{3-\delta}(n-\delta)}. \tag{2.21}$$

Furthermore, we express it using energy and the equation 2.18, we get

$$E_{\text{ej}} = E_{\text{in}} + E_{\text{out}} = \frac{4\pi B_{\text{in}} v_{\text{tr}}^{5-\delta}}{2(5-\delta)(n-5)}. \tag{2.22}$$

Moreover, involving the inner density coefficient, we get

$$B_{\text{in}} = \frac{2E_{\text{ej}}(5-\delta)(n-5)}{4\pi v_{\text{tr}}^{5-\delta}(n-\delta)}. \tag{2.23}$$

If we compare equations 2.21 and 2.23 we get the velocity of the transition region,

$$v_{\text{tr}}^2 = \frac{2E_{ej}}{M_{ej}} \left(\frac{(5-\delta)(n-5)}{(3-\delta)(n-3)} \right). \tag{2.24}$$

Since we got an analytical solution for transitional velocity, it is possible to explicitly express analytical equations for densities at given distance and time. However, for studying interaction, we need to add the circumstellar medium with the assumption that density can be quantified as a power law

$$\rho_{\mathrm{csm}} = Dr^{-s}. \tag{2.25}$$

We make a condition for s to be smaller than 3, for later integration.[6] Then to calculate the mass of the shocked ejecta of the SN, we must integrate each region separately [7],

$$M_{\mathrm{sh}} = \int_{v_{\mathrm{sn}}t}^{v_{\mathrm{max,\,sn}}t} 4\pi r^2 \rho_{\mathrm{out}} dr + \int_{R_{\mathrm{s}}}^{r_{\mathrm{sh}}} 4\pi r^2 \rho_{\mathrm{csm}} dr, \tag{2.26}$$

where R_{s} is the radius of the progenitor, v_{sn} the velocity of the ejecta and $v_{\mathrm{max,\,sn}}$ is the maximal velocity of the outermost layer in time of interaction. We assume that $r_{\mathrm{sh}} \gg R_s$ and $v_{\mathrm{max,\,sn}} \gg v_{\mathrm{sn}}$. After substituting densities from equations 2.25, 2.12, and after some arrangements, we get

$$M_{\mathrm{sh}} = \frac{4\pi B_{\mathrm{out}} t^{n-3}}{3-n}\left[r^{-n+3}\right]_{v_{\mathrm{sn}}}^{v_{\mathrm{max,\,sn}}} + \frac{4\pi D}{3-s}\left[r^{-s+3}\right]_{R_{\mathrm{S}}}^{r_{\mathrm{sh}}},$$

$$M_{\mathrm{sh}} = \frac{4\pi B_{\mathrm{out}}}{n-3}\left(\frac{t}{r_{\mathrm{sh}}}\right)^{n-3} + \frac{4\pi D}{3-s} r_{\mathrm{sh}}^{3-s}. \tag{2.27}$$

We apply the conservation of momentum, which must be fulfilled for the thin shocked shell. However, the Rankine-Hugoniot conditions 2.7 are for the coordinate frame co-moving with discontinuity, and we "are" now in the rest frame, so we include this by expressing the velocity relative to discontinuity.

$$\rho_{\mathrm{sn}}(v_{\mathrm{sn}} - v_{\mathrm{sh}})^2 - \rho_{\mathrm{csm}}(v_{\mathrm{sh}} - v_{\mathrm{w}})^2 = \frac{M_{\mathrm{sh}}}{4\pi r_{\mathrm{sh}}^2}\frac{dv_{\mathrm{sh}}}{dt}, \tag{2.28}$$

where

$$v_{\mathrm{sn}} = \frac{r_{\mathrm{sh}}}{t},\ v_{\mathrm{sh}} = \frac{dr_{\mathrm{sh}}}{dt}. \tag{2.29}$$

The velocity of thin dense shell is v_{sh} and the velocity of the CSM (or wind) is v_{w} is. Substituting M_{sh} from equation 2.27, and expressing the densities from equations 2.25 and 2.12, with assumption that the velocity of the wind can be neglected ($v_{\mathrm{sh}} \gg v_{\mathrm{w}}$) and using simple relation between velocity and radius 2.29, we get

$$4\pi r_{\mathrm{sh}}^2 B_{\mathrm{out}} \frac{t^{n-3}}{r_{\mathrm{sh}}^n}\left(\frac{r_{\mathrm{sh}}}{t} - \frac{dr_{\mathrm{sh}}}{dt}\right)^2 - 4\pi D r_{\mathrm{sh}}^2 r_{\mathrm{sh}}^{-s}\left(\frac{dr_{\mathrm{sh}}}{dt}\right)^2 =$$

$$= \left[\frac{4\pi B_{\mathrm{out}}}{n-3}\left(\frac{t}{r_{\mathrm{sh}}}\right) + \frac{4\pi D}{3-s} r_{\mathrm{sh}}^{3-s}\right]\frac{d\left(\frac{r_{\mathrm{sh}}}{dt}\right)}{dt}. \tag{2.30}$$

If we assume that the solution for radius of the thin shocked shell is a power law in the form $r_{\mathrm{sh}}(t) = At^{\alpha}$, we can solve the differential equation 2.30. We get a solution

[6] This condition is possible to obtain self-similar assumption [9], [10].

[7] The outer part of the star and region with CSM.

$$A^{n-s}\frac{D}{B_{\rm out}}\frac{\frac{\alpha(\alpha-1)}{3-s}+\alpha^2}{(1-\alpha)^2+\frac{\alpha(1-\alpha)}{n-3}}=t^{n-3-\alpha(n-s)}=const. \tag{2.31}$$

The power must equal to the zero and this implies $\alpha=(n-3)/(n-s)$. Moreover, after substituting the α to equation 2.31, and expressing the parameter A, we get the explicit solution for the radius of the shock wave

$$r_{\rm sh}=\left[\frac{(3-s)(4-s)}{(n-3)(n-4)}\frac{B_{\rm out}}{D}\right]^{1/(n-s)}t^{(n-3)/(n-s)}. \tag{2.32}$$

Moreover, this is the same time-dependent solution as from self-similar assumptions for example in [9]. This equation applies if the interacting region reaches inner ejecta region, so when the expanding ejecta velocity $v_{\rm sn}$ enters the thin shocked shell, it would be equal to $v_{\rm tr}$ or $r_{\rm sh}(t_{\rm tr})=v_{\rm tr}t_{\rm tr}$. Combining equations 2.24 and 2.32, we get the time of the transition

$$t_{\rm tr}=\left[\frac{(3-s)(4-s)}{4\pi D(n-\delta)(n-3)}\frac{[(3-\delta)(n-3)M_{\rm ej}]^{(5-s)/2}}{[2(5-\delta)(n-5)]^{(3-s)/2}}\right]^{\frac{1}{3-s}}. \tag{2.33}$$

2.3 Analytical solution of bolometric light curves

We demonstrate analytical solution of bolometric light curve as it is shown in [33]. The assumption for deriving is that the main power source is a conversion of ejecta kinetic energy of SN to the dense CSM. We consider that CSM is transparent for radiation,

$$dE_K=\frac{1}{2}v_{\rm sh}^2dm_{\rm sh}=\frac{1}{2}v_{\rm sh}^2 4\pi r_{\rm sh}^2\rho_{\rm csm}dr_{\rm sh}=2\pi r_{\rm sh}^2\rho_{\rm csm}dr_{\rm sh} \tag{2.34}$$

where we include new parameter $\varepsilon_{\rm L}$, which is coefficient for conversion efficiency of the kinetic energy

$$L=\varepsilon_{\rm L}\frac{dE_{\rm K}}{dt}=2\pi\varepsilon_{\rm L}\rho_{\rm csm}r_{\rm sh}^2v_{\rm sh}^2\frac{dr_{\rm sh}}{dt}. \tag{2.35}$$

The radius of the shock $r_{\rm sh}$ is given by eq. 2.32, this holds for time before transition time $t_{\rm tr}$, see eq. 2.33. We can express the luminosity as a power law

$$L=L_0t^{\beta}, \tag{2.36}$$

where L_0 and β can be expressed as

$$L_0=2\pi\varepsilon_{\rm L}D\left(\frac{n-3}{n-s}\right)^3\left[\frac{(3-s)(4-s)}{(n-3)(n-4)}\frac{B_{\rm out}}{D}\right]^{(5-s)/(n-s)},\ \beta=\frac{2n+6s-ns-15}{n-s}. \tag{2.37}$$

This means that bolometric LCs can be fitted with two constants L_O and β, this means that numerical model without this type of function can shows us discrepancy between numerical and analytical model.

2.4 Modules for Experiments in Stellar Astrophysics - MESA

2.4.1 Introduction

Modules for Experiments in Stellar Astrophysics (**MESA**)[40][41] is a package of modules that can be applied and used in a variety of simulations and problems in the stellar astrophysics. Each of these modules is open source, efficient and thread-safe[8], which provides the possibility to use modern computers effectively. The programming language chosen for MESA modules is *Fortran 95*, and each one of the modules is standalone. This feature makes MESA suitable not only for stellar evolution but also to solve different stellar physics problems as it contains options to modify input parameters easily. Physical modules are, for example, the ones used to calculate the equation of the state, opacity or nuclear reaction network, or they can be numerical, i.e., matrix solvers or interpolation routines. MESA star is a one dimensional (1D) stellar evolution module with modern numerical methods and physics. MESA star is designed to consistently solve even the complicated stages of star evolution, such as helium burning in less massive stars. This caused problems for stellar evolution codes in the past. Firstly it reads input files, then creates a nuclear reaction network in RAM and access to the equation of the state and opacities data. MESA star runs in four steps: 1. MESA prepare to take new timestep and can re-mesh model if necessary. 2. It alters model with the change in the mass caused by stellar wind or accreted mass. In this step, it is also included that it changes abundances, calculate convective diffusional coefficient, and solves new structure and composition with the Newton-Raphson solver. 3. MESA estimate next timestep. 4. Lastly, the output is generated and continues in the loop until a requirement for the ending is met.

MESA code can start even in pre-main sequence star and let it collapse to MS star; however, MESA shows good convergence for the pre-MS star only in the initial mass range of $0.02 - 50\,M_{\odot}$.

2.4.2 Microphysics

Microphysics is divided into three different processes, and for each process, MESA star uses a separate module. First one is a module for treating nuclear reactions (how much energy is radiated). The heat deposited to surrounding material is calculated from differences in nuclear masses from JINA Recalib database and include energy losses by weak neutrinos which are effectively radiated away. This module includes a one-zone burning routine which is applied to the defined initial chemical composition. The second module is the equation of the state (EoS). EoS is calculated from two independent variables: ρ and T. These two variables are essential for the calculation of Helmholtz free energy. However, sometimes it is easier to calculate EoS from P and T; these are essential variables for Gibbs free energy formulation of thermodynamics. The MESA ρ-T table is based on OPAL EoS tables made by Rogers & Nayfonov in 2002 [42].

Next, we briefly mention the problem of convection in MESA[9]. Convection is treated by

[8] MESA is using OpenMP to do the parallel calculation of local micro-physics.

[9] It is int interesting that similar problem is even in SN explosion.

the module mlt (mixing length theory) in the MESA. Mlt calculates diffusional coefficient because it treats the mixing element as a diffusional process. However, convective mixing is not enough when the code is only in spherical symmetry. It is needed to include convective overshooting mixing, which is process when an essential element in the star has enough kinetic energy to exceed condition given only from only convective mixing theory. It is possible to vary this coefficient during different phases of the evolution of the star, i.e., nonburning, H-burning or He burning.

2.5 SuperNova Explosion Code - SNEC

2.5.1 Introduction

SNEC (SuperNova Explosion Code)[35] is open-source, Lagrangian code for solving hydrodynamics and radiation transport in core-collapse supernovae. Besides, it includes the effects of decaying radioactive Ni. Output data from SNEC can either be bolometric lightcurve or lightcurve in different wavebands.

In each time step, SNEC calculates equations for mass conservation, and momentum conservation and energy conservation in the explicit form.

$$\frac{\partial r}{\partial m} = \frac{1}{4\pi r^2 \rho},$$

$$\frac{\partial v}{\partial t} = -\frac{Gm}{r^2} - 4\pi r^2 \frac{\partial P}{\partial m} - 4\pi \frac{\partial (r^2 Q)}{\partial m},$$

$$\frac{\partial \varepsilon}{\partial t} = \frac{P}{\rho}\frac{\partial \rho}{\partial t} - 4\pi r^2 \frac{\partial v}{\partial m} - \frac{\partial L}{\partial m} + \varepsilon_{\mathrm{Ni}}.$$

Here, m is the mass coordinate, r is the radius, t is the time, ρ is the mass density, ε is the specific internal energy, P is the pressure, Q is the artificial viscosity, $\varepsilon_{\mathrm{Ni}}$ is the energy deposited by decaying nickel, and G is the gravitational constant.

2.5.2 Input and parameters

SNEC's input data and parameters can be easily changed. The data are in the main directory named *profile*, where the input data must meet some of the requirements of arranging the progenitor data. Parameters are mainly in the text file named *parametrs* in the SNEC main directory. It is good to know, that if we want to change some parameters, we only need to change values.

SNEC provides two equations of state in the newest version. First one is the ideal single particle Boltzmann gas EOS; however, it mainly serves for test purposes, specifically for the Sedov blast wave test. However, we used Paczynski equation of state, which is simplified EoS used analytically for ions, photons, and semi-relativistic electrons. SNEC allows distributing nickel into the star to the maximum boundary defined by the mass coordinate.

The chemical composition in the progenitor is changing abruptly at minimal distances. In the supernovae event, it is probably caused by Rayleigh-Taylor instabilities, during transition shockwave; however, to model such instability, we would need a 3D model

with high-resolution mesh. So, the steep gradients in chemical composition are in SNEC smoothed by the so-called boxcar smoothing, the subroutine in the SNEC, which helps to smooth the composition of the progenitor star and imitate instabilities by mixing chemical composition within a local area.

Chapter 3

Modelling and Results

3.1 Method

We use similiar method as in [4] and [36]; but with some differences.

We created the script (Appendix A), which stitches the dense CSM to the progenitor and transform coordinates (noting that MESA primarily needs to input the Lagrangian mass coordinate while SNEC code is Eulerian, that is, the coordinate system used is spatial), so we can input the data to SNEC. After this, we explode progenitor with CSM in SNEC with thermal bomb type explosion, which adds the energy just above the region where the proto-NS has been formed. Moreover, we have compared our calculations with observed data as well as with calculated models of some authors. In this section, we describe in more detail, the parameters used in each step.

3.1.1 MESA

We selected for our progenitor a pre-main sequence star with mass $12 M_{\odot}$ for all our SN simulations. The star is then evolved with Modules for Experiments in Stellar Astrophysics, **MESA** (release 10398) [40]. We initialized this model with metallicity $Z = 0.02$ and solar abundances distribution. The model evolved without rotation nor with the mass-loss through winds. The model is evolved from pre-MS to core collapse, which is defined as a terminal condition in time when the infall velocity of any region reaches $\geq 1000\,\mathrm{km\,s^{-1}}$. We use **MESA** inlist and the approx21_cr60_plus_co56 nuclear burning network available from [15] as well as the time and resolution scheme during different burning phases, which leads to pre-SN model.

While the mass-loss mechanism affects the final mass of the progenitor significantly, we did not include any wind. We can see the density and temperature profile of the pre-supernova in figure 3.1.

3.1.2 Script - Appendix A

We create a script (Appendix A) for stitching dense CSM to the progenitor. The script takes the output data from MESA, adjust them to be readable for SNEC, and join the progenitor with dense CSM. We assume CSM to be a spherically stellar wind with a density profile

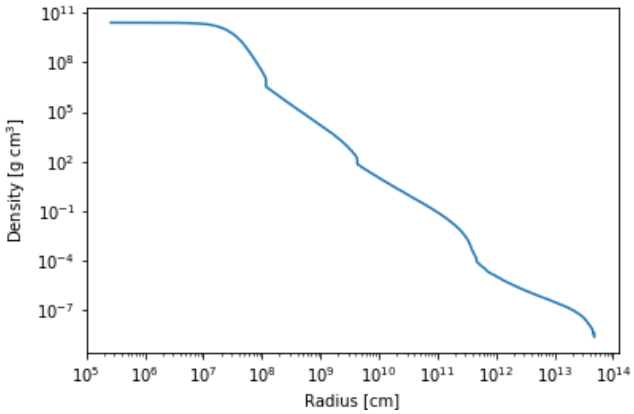

(a) The density profile of the progenitor.

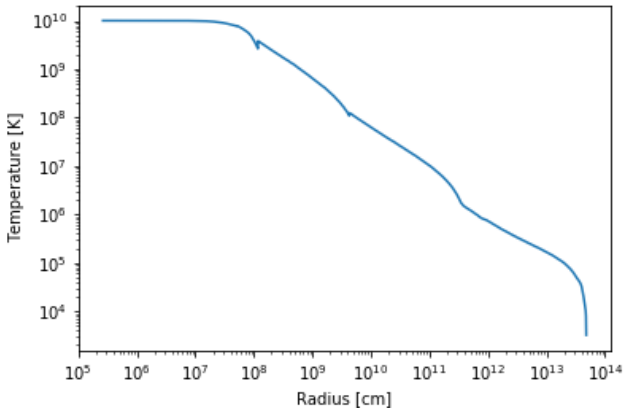

(b) The temperature profile of the progenitor.

Figure 3.1: Profile of the pre-SN progenitor with 12M$_\odot$. On both horizontal axes is the radius.

derived from the mass continuity equation as follows

$$\rho_{csm}(\mathrm{r}) = \frac{\dot{M}}{4\pi r^2}\frac{1}{v(\mathrm{r})}, \tag{3.1}$$

where $\dot{M}$ is the selected mass loss rate (free parameter), r radius and $v(\mathrm{r})$ is the wind velocity. The density profile of the CSM abruptly changes to zero at a distance of radius $1500\,R_\odot$ (after the surface of the star). We choose this radius because it is almost in agreement with [36], and because this parameter has little effect on CSM mass when $\beta \geq 3$. We assumed the velocity profile to obey the beta law

$$v(r) = v_0 + (v_\infty - v_0)\left(1 - \frac{R_*}{r}\right)^\beta, \tag{3.2}$$

where v_0 is the velocity on the stellar surface, v_∞ is the terminal velocity, and β is the parameter describing the steepness velocity. This equation differs from classical so-called

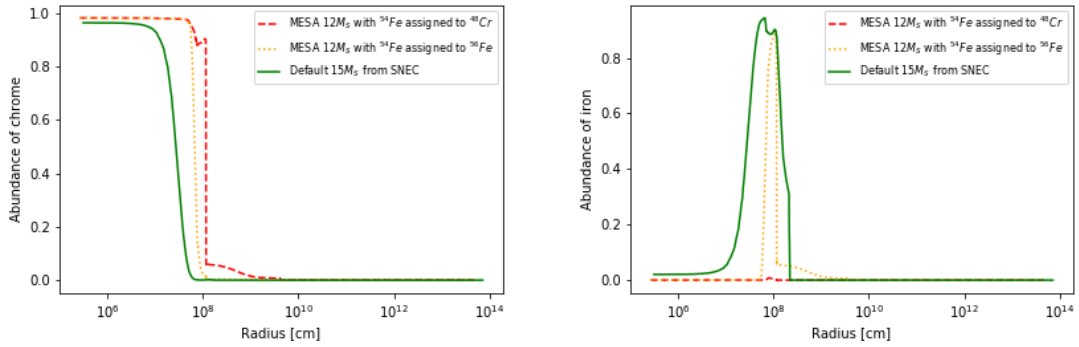

(a) Chrome abundance profile in the progenitor. (b) Iron abundance profile in the progenitor.

Figure 3.2: Abundances of chrome and iron in the progenitor, and graphical visualization of choosing where to assign specific isotope of ^{54}Fe. We choose the orange line (assign ^{54}Fe to ^{56}Fe), shows a similar trend on the right graph as our representative model shown with a green line. The difference can be caused by the heavier mass of the progenitor (green line) produce more iron. Secondly, we used the bigger nuclear burning network (red and orange lines), which probably caused the different abundance structure.

velocity law so that the velocity would be a continuous function on the surface of the progenitor, similar as is in [4]. In our model we assumed $v_\infty = 10\,\mathrm{km\,s^{-1}}$, unless it is stated otherwise. The same velocity was used in other models such as [34], [36]. Moriya et al. in [34] even concluded that velocity has little impact on the LC.

We unlock the following parameters in MESA to be printed out in output data, namely radial velocity and electron fraction. This has to be due to the SNEC requirements for the input. For printing out, it is needed to modify the file in the

$\$MESA\_DIR\$/star/defaults/profile\_columns.list$.

SNEC tables do not cover entirely all chemical isotopes generated from MESA nuclear burning network, and we would need to assign the chemical isotopes not covered by SNEC to the most similar ones. As an example, we used a default profile of RSG with (ZAMS) mass $15\,M_\odot$ in SNEC default folder, which was evolved with MESA. If the given element (for example ^{3}He in MESA) was only a trace amount, we assigned then to similar isotopes (^{3}He with two neutrons to ^{4}He with two neutrons). The analysis was done only for isotopes, which may affect the calculations. For example, the reason for merging ^{54}Fe to ^{52}Fe and not to chrome ^{48}Cr is shown on figure 3.2.

Since the CSM is dense, the photosphere is expected to be in the CSM, which is certainly heated. For that reason, we used the assumption that effective temperature and the composition is the same as on the surface of the star.

3.1.3 SNEC

SNEC assumes that the innermost part of the star with $1.4M_\odot$[1] is left out to form the NS, and this part of the star is omitted in the explosion. We choose the type of the explosion

[1] It is possible to change this value.

to be a thermal bomb to which applies energy to the innermost region, above the mass cut. Thermal bomb implemented by SNEC gives a few more percent energy to the system; however, it was found out that it conserves total energy past 150 days after explosion [36]. The composition is smoothed with "boxcar", to simulate element mixing which is caused during the explosion. In our model generated from MESA, we get mass of the Ni $0.01 M_{\odot}$, however in this amount is not included nickel generated by r-process during SN explosion. Due to this, we input the mass of Ni to be $0.05 M_{\odot}$ for all of our models. This mass of the nickel is consistent with [25], where they concluded that expected mass of the Ni in SN II-P is expected in the range $\approx 0.01 - 0.1 M_{\odot}$. Ni is distributed in the region between the Lagrangian coordinate $1.4 M_{\odot}$ up to $4 M_{\odot}$ and. We use default opacity tables and Paczynski EoS as included in the SNEC.

3.2 Test models

Firstly we create test models to find out how parameters affect the light curve. Experimental models are in figure 3.4. We mentioned earlier that SN interaction with CSM is not very dependant on velocity of the CSM [36] and work of Moriya et al. [34] concludes that effects of different progenitor (RSG) models inside the CSM are not very significant.

From testing models, we selected parameters which mainly affect LCs: The energy of the explosion, the mass loss rate, and β parameter. We noticed from the bolometric LC that most important was not the mass loss rate or β, but the total mass of the CSM.3.4 The table 3.3 is for showing the total mass of the CSM as a primary free parameter; however, the mass of the CSM has a different structure.

Our testing models have energies between $0.6 - 1.2 \times 10^{51}$ erg with 0.2×10^{51} erg step (4 steps) and the mass of the CSM between $0 - 1.64 M_{\odot}$ (10 steps 3.3) and so the mesh of testing models consists from 40 models of SNe.

We defined χ as

$$\chi^2 = \sum_{\lambda \in (\mathrm{V,\,R})} \sum_{\mathrm{t}^* < \mathrm{t_{plt}}} \frac{(M^*_\lambda(t^*) - M_\lambda(t^*))^2}{M^*_\lambda(t^*)}, \tag{3.3}$$

where t^* is time observed, $M^*_\lambda(t^*)$ is the observed magnitude at observed time, while $M_\lambda(t^*)$ is the calculated magnitude in observed time, and $\mathrm{t_{plt}}$ is understimated length of the plateau which can be seen in LC.[2]

We evaluated model based on their χ, and we choose the lowest χ in the script, which fix the observed data and move calculated data while is calculating χ in every step. The script includes observed light curve in V and R waveband in a period of 5 days before maximum in V waveband and 65 days after maximum. We choose wavebands included in χ to be V and R waveband because B and more bluer waveband are affected by elements from the iron group by line blanketing [25], and we did not include redder waveband because we did not use any reddening correction.

For our work, we selected three well observed SN with RSG progenitor and observed a narrow component in H. In figures 3.10a - 3.10c we would use energy unit **foe** (**f**ifty **o**ne **e**rgs 1 foe $= 10^{51}$ erg, and chi-squared χ^2.

[2] We choose 65 days. In [36] they calculate it for SN2013fs on 83 days, and for SN2013ej on 99 days.

	$\beta = 1$	$\beta = 3$	$\beta = 5$
$10^{-3} M_{\odot}/yr$		$0.08 M_{\odot}$	$0.16 M_{\odot}$
$5 \times 10^{-3} M_{\odot}/yr$		$0.39 M_{\odot}$	$0.82 M_{\odot}$
$10^{-2} M_{\odot}/yr$	$0.12 M_{\odot}$	$0.78 M_{\odot}$	$1.64 M_{\odot}$
$5 \times 10^{-2} M_{\odot}/yr$	$0.61 M_{\odot}$		
$10^{-1} M_{\odot}/yr$	$1.22 M_{\odot}$		

Figure 3.3: Mass of the CSM in different models, later we noticed that the LC was the most affected by the total mass and in later figure we are using only the mass of the CSM.

To search for data, we use The Open Supernova Catalog[18] to download data as CSV file. From this catalog, we apply distance modulus for selected SN.

3.3 SN 2011ht

SN 2011ht was very weak SN with maximum absolute magnitude only 17.4^{mag}, in one time it was even labeled as an imposter. The mass of the Ni is very low at $\approx 0.006 - 0.01 M_{\odot}$. Due to the very low radiated energy $2 - 3 \times 10^{49}$ erg, progenitor is assumed to be a star with $8 - 10 M_{\odot}$, which undergoes core collapse, or it could be the star $\geq 25 M_{\odot}$ with a fallback of metal-rich ejecta [32]. We selected this SN, although SN was probably EcSN so we could see if our model would falsely identify the mass and the energy. Our tests models did not cover explosion energy or mass of the CSM estimated by work [11]. However, the progenitor is expected to be RSG, which is similar to the one used in the model.

We use distance modulus equal to 30.99^{mag} for our analysis, that is taken from [5] and [18]. The observed data are taken from [5] and [32].

The fitting values of our models can be seen in figure 3.10a. We compare our best-fitting model with work of N. N. Chugai[11]; however, He assumed in his work that the energy of the explosion is $\approx 6 \times 10^{49}$erg and mass of the CSM is assumed to be $6 - 8 M_{\odot}$. We get the best fit for the energy of explosion 6×10^{50} erg for a model without the CSM. However, our model can not predict the time, when the explosion happens because χ^2 is increasing when it is getting close to the presumable explosion time. The fit with lowest χ^2 is shown in figure 3.5. We see from the LC that calculated curve has a very different shape. The lowest fit is due to the modelled LC crossing through observed data, which artificially decrease χ^2, and not because it was closest to SN 2011ht.

3.4 SN 2013ej

We use distance modulus for this SN, that is equal 29.9^{mag} [8], [22]. Observed data are taken from [22], [60] and [5].

According to the work [36], the best fitting model for this SN has progenitor's mass $12.5 M_{\odot}$ (noting we used progenitor with $12 M_{\odot}$), explosion energy is 0.6×10^{51} erg and mass of the CSM is roughly $0.624 M_{\odot}$. Our best fitting model have energy of the explosion 0.6×10^{51} erg and the mass of the CSM is roughly $0.82 M_{\odot}$ from 3.10b- The LC of the best model is shown in figure 3.6.

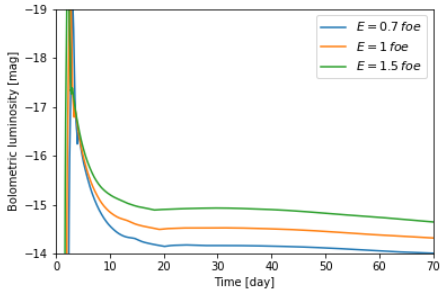

(a) Various initial energy.

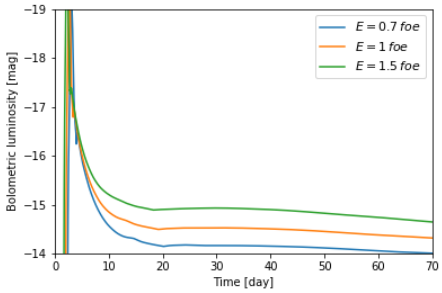

(b) Various initial energy.

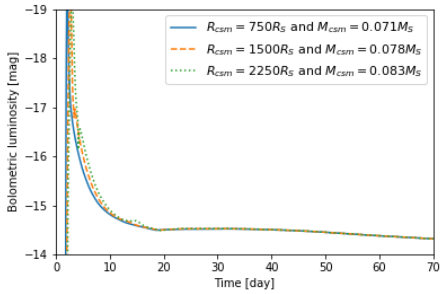

(c) Various length of the CSM.

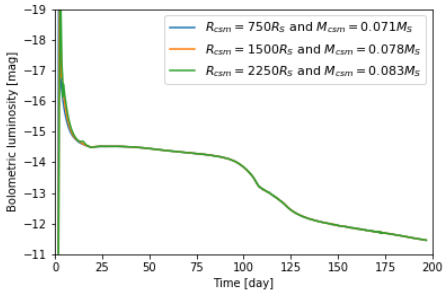

(d) Various length of the CSM.

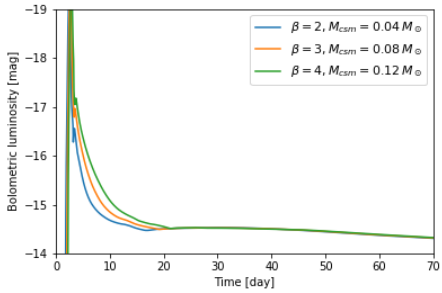

(e) Different beta laws.

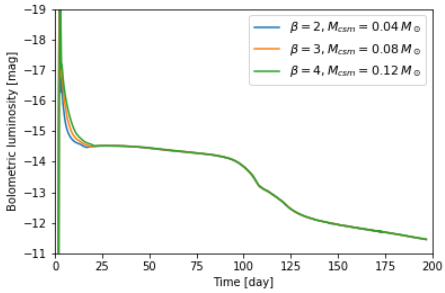

(f) Different beta laws.

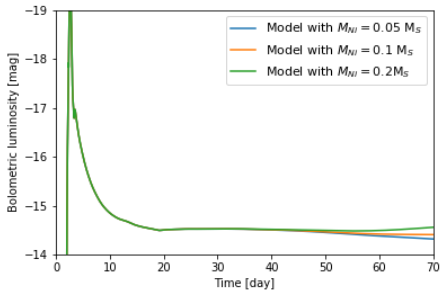

(g) Various initial mass of the nickel.

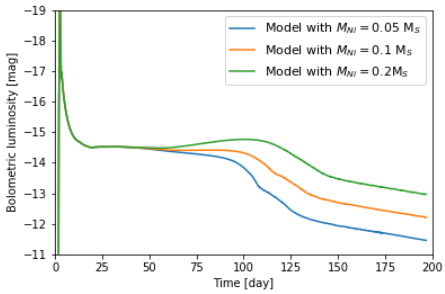

(h) Various initial mass of the nickel.

Figure 3.4: Test models with different parameters. If not specified otherwise test model is progenitor $12\,M_\odot$ with the CSM $M_{\rm csm} = 0.08\,M_\odot$ (β= 3, $\dot{M} = 10^{-3}\,M_\odot\,yr^{-1}$). Figures on the right are during plateau phase.

.

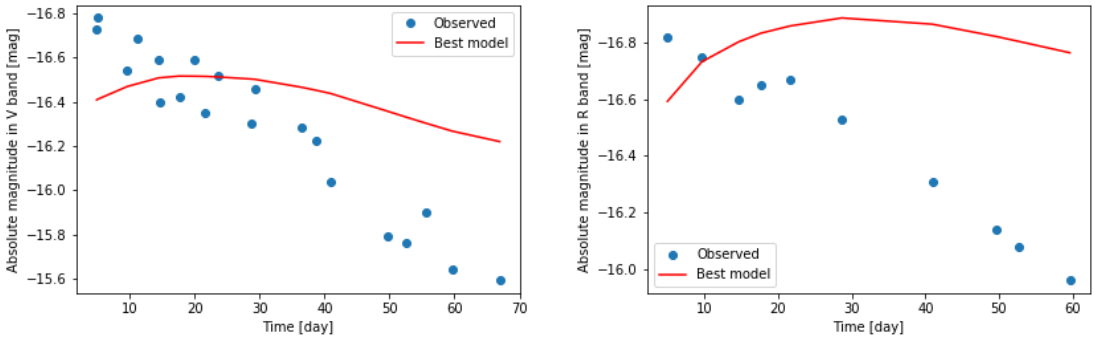

(a) V - waveband (b) R - waveband

Figure 3.5: LC of SN 2011ht. Model is $E = 0.6$ foe without CSM is the red line, observed data are blue dots.

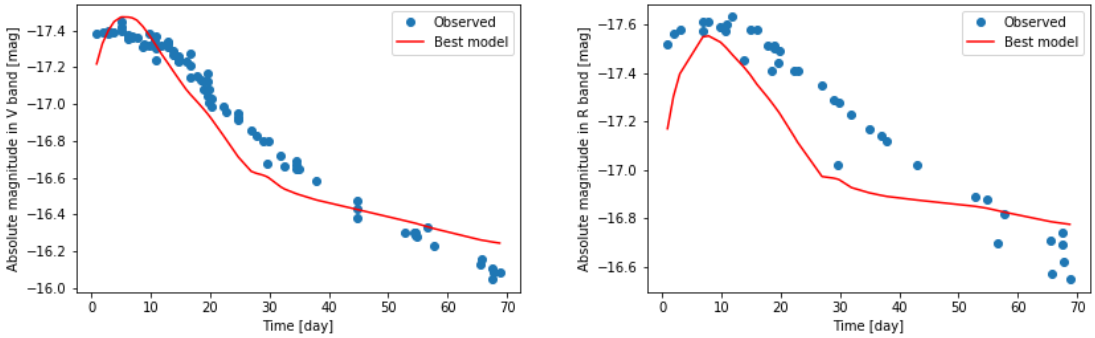

(a) V- waveband (b) R- waveband

Figure 3.6: LC of SN 2013ej. Model is $E = 0.6$ foe with $M_{\rm csm} = 0.82\,M_{\odot}$ is the red line, observed data are blue dots.

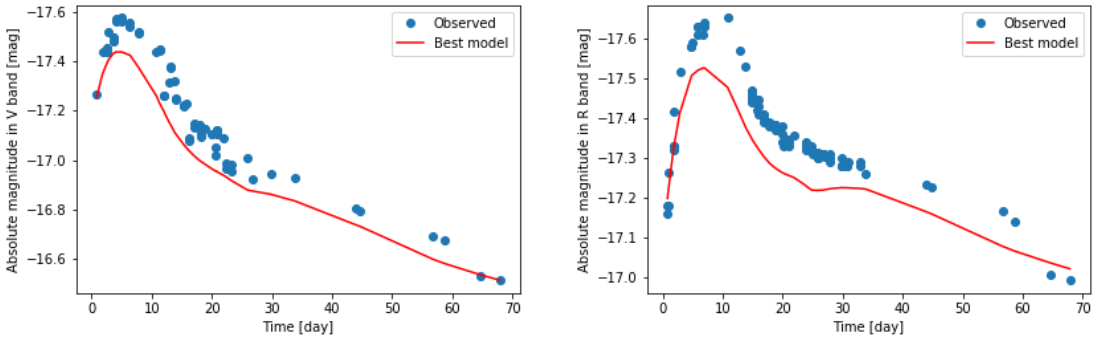

(a) V- waveband (b) R- waveband

Figure 3.7: LC of SN 2013fs. Model is $E = 0.6\,\text{foe}$ with $M_{\text{csm}} = 0.61\,M_{\odot}$ is the red line, observed data are blue dots.

3.5 SN 2013fs

The distance modulus for SN 2013fs is 33.54^{mag} [18], [5]. Observed data are taken from [44], [55] and [5].

According to the [36], the best fitting model is progenitor with mass $12.5\,M_{\odot}$, energy of the explosion 0.8×10^{51} erg and the mass of the CSM is roughly $0.5\,M_{\odot}$. Our work obtains more than one good fit. The first model with the best fit is shown in 3.7. The second model is similar to the first one, but the mass of the CSM is higher than in the first model, and the LC is shown in figure 3.8. The third model is similar to the work of [36]. The explosion energy is 0.8×10^{51} erg and mass is equal to $0.39\,M_{\odot}$ (the mass of our progenitor is $12\,M_{\odot}$). The LC for this model is shown in figure 3.9.

We can see from LCs that correct model is probably the last one, due to many observations done in the middle of LC, which caused that good fit of the middle part of the LC decreases χ^2. The first model is similar to the third one, but calculated luminosity is underestimated at every point in the peak. This could be improved with better data processing.

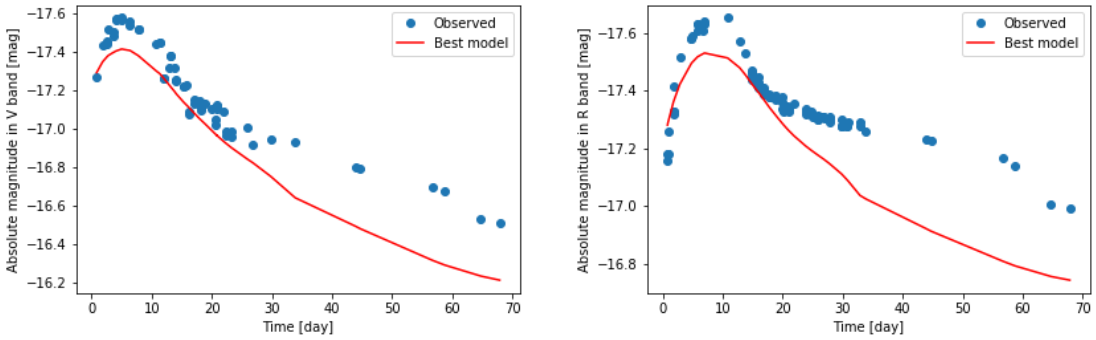

(a) V- waveband (b) R- waveband

Figure 3.8: LC of SN 2013fs. Model is $E = 0.6\,\text{foe}$ with $M_{\text{csm}} = 0.82\,M_{\odot}$ is the red line, observed data are blue dots.

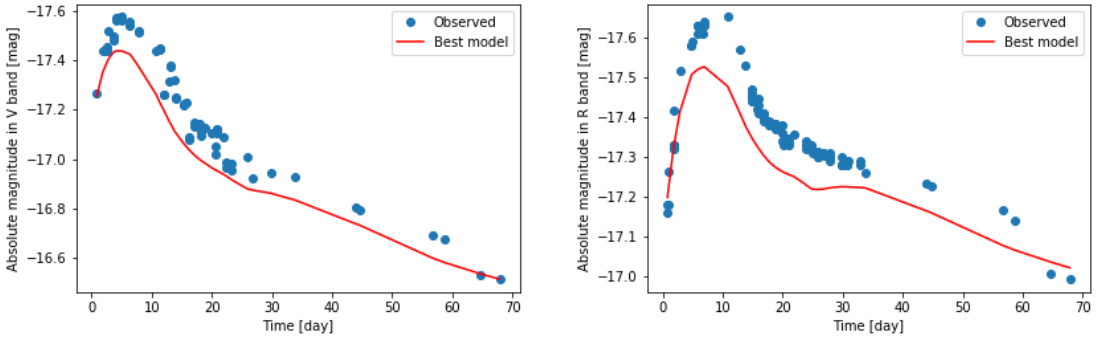

(a) V- waveband (b) R- waveband

Figure 3.9: LC of SN 2013fs. Model is $E = 0.8\,\text{foe}$ with $M_{\text{csm}} = 0.39\,M_{\odot}$ is the red line, observed data are blue dots.

SN 2011ht	E = 0.6 foe	E = 0.8 foe	E = 1 foe	E = 1.2 foe
Without CSM	0.49	0.96	1.51	2.06
$M_{csm} = 0.08 M_{\odot}$	0.49	0.99	1.56	2.15
$M_{csm} = 0.12 M_{\odot}$	0.49	0.99	1.57	2.15
$M_{csm} = 0.16 M_{\odot}$	0.52	1.07	1.67	2.27
$M_{csm} = 0.39 M_{\odot}$	0.62	1.23	1.89	2.52
$M_{csm} = 0.61 M_{\odot}$	0.87	1.58	2.30	2.98
$M_{csm} = 0.78 M_{\odot}$	0.83	1.54	2.26	2.94
$M_{csm} = 0.82 M_{\odot}$	0.99	1.76	2.51	3.23
$M_{csm} = 1.22 M_{\odot}$	1.29	2.14	2.96	3.72
$M_{csm} = 1.64 M_{\odot}$	1.37	2.25	3.09	3.87

(a) SN 2011ht

SN 2013ej	E = 0.6 foe	E = 0.8 foe	E = 1 foe	E = 1.2 foe
Without CSM	2.68	1.52	1.40	1.79
$M_{csm} = 0.08 M_{\odot}$	2.09	1.16	1.19	1.69
$M_{csm} = 0.12 M_{\odot}$	1.79	1.05	1.18	1.70
$M_{csm} = 0.16 M_{\odot}$	1.13	0.76	1.06	1.72
$M_{csm} = 0.39 M_{\odot}$	0.58	0.59	1.16	2.05
$M_{csm} = 0.61 M_{\odot}$	0.26	0.72	1.68	2.86
$M_{csm} = 0.78 M_{\odot}$	0.28	0.66	1.57	2.72
$M_{csm} = 0.82 M_{\odot}$	0.20	0.85	1.98	3.31
$M_{csm} = 1.22 M_{\odot}$	0.35	1.45	2.91	4.47
$M_{csm} = 1.64 M_{\odot}$	0.40	1.51	3.01	4.62

(b) SN 2013ej

SN 2013fs	E = 0.6 foe	E = 0.8 foe	E = 1 foe	E = 1.2 foe
Without CSM	3.1	1.4	0.96	1.15
$M_{csm} = 0.08 M_{\odot}$	2.23	0.86	0.65	0.96
$M_{csm} = 0.12 M_{\odot}$	2.00	0.73	0.53	0.86
$M_{csm} = 0.16 M_{\odot}$	1.31	0.37	0.41	0.93
$M_{csm} = 0.39 M_{\odot}$	0.63	0.19	0.59	1.38
$M_{csm} = 0.61 M_{\odot}$	0.16	0.42	1.28	2.40
$M_{csm} = 0.78 M_{\odot}$	0.20	0.36	1.19	2.31
$M_{csm} = 0.82 M_{\odot}$	0.16	0.68	1.76	3.09
$M_{csm} = 1.22 M_{\odot}$	0.40	1.45	2.91	4.50
$M_{csm} = 1.64 M_{\odot}$	0.40	1.47	2.99	4.66

(c) SN 2013fs

Figure 3.10: The red colour is reserved for $\chi^2 < 0.30$, the yellow $0.30 \leq \chi^2 < 0.6$ and green $0.6 \leq \chi^2$; however we are using blue colour if the χ^2 is increasing around the SN explosion.

Conclusion

The primary purpose of this thesis was to understand and make a model of an SN interacting with the CSM and to compare it with the observed LCs of SNe, as well as with the models of other authors.

The first chapter is the overview for a better understanding of the complexity of the SN problem, and it summarizes many physical processes that occur during and after the explosion. The second chapter is focused mainly on an explanation of the interaction between the SN and the CSM as well as the software used in this work. The core of this thesis is the third chapter, in which we use both the MESA software package for the evolution and SNEC package for the explosion of the star.

We investigate numerically the LCs of three chosen SNe with well known red RSG progenitors and the interactions with the CSM. Figures 3.5, 3.6 and 3.9. The best fit for the LC of the SN 2011ht was not satisfactory; however, this is an expected outcome, as the mesh of the models does not cover the calculated energy range of the explosion, nor the mass of the CSM. In the case of SN 2013ej and SN 2013fs, the best fits for LCs were satisfactory. The models were compared with the models of other authors, and the results were found to be similar.

The difference between the observed LCs and the models are probably due to the spherical symmetry approximation. Additionally, the SNEC approximates the model as a blackbody, and we make many approximations during the addition of the CSM to the progenitor. Moreover, lastly but importantly, the density profile of the CSM is still not well known.

This work still confirms that the CSM affects the LC of the SN, of which the parameters with the most significant impact on the LC are the mass loss and β. However, even for the steepest density profile $\beta = 5$ we do not reach satisfactory LC without mass loss much higher than the typical wind of RSG. Typical mass loss of the RSG is $10^{-4} M_{\odot}\,\mathrm{yr}^{-1}$ [47].

Appendix A

For correct function these codes have to be with two folder named exactly **MESA** and **SNEC**. In folder named **MESA** must be two files one is **final_model.mod** which is copied from output from MESA main folder and second one is called **profile.data**, which is copied from LOGS in MESA main folder and renamed to only profile without number.[3]

```
import numpy as np
import mesa_reader as mr
import os

#CGS value for constants
M_Sun = 1.99*10**33
R_Sun = 6.96*10**10

#Loading models
p_M = mr.MesaData('MESA/profile.data')
f_M = mr.MesaData("MESA/final_model.mod")


#Deleting old copies if they exist before it may cause
#otherwise problems with close()
if os.path.exists("SNEC/profile.short"):
    os.remove("SNEC/profile.short")
else:
    print("Neexistuje súbor .short")
if os.path.exists("SNEC/profile.iso.dat"):
    os.remove("SNEC/profile.iso.dat")
else:
    print("Neexistuje súbor iso dat")
p_S = open("SNEC/profile.short", "w+")
f_S = open("SNEC/profile.iso.dat", "w+")

#Constant for dividing wind or CSM
wind_num = 300
#Create SNEC profile
num = p_M.num_zones
```

[3] It is possible to command MESA to named final profile as profile.data which is alternative methods.

```
p_S.write("%d\n" % (num+wind_num))
#Load MESA data
a = p_M.data("mass")
b = p_M.data("logR")
c = p_M.data("logT")
d = p_M.data("logRho")
e = f_M.data("v")
#e = p_M.data("velocity")
f = p_M.data("ye")
g = p_M.data("omega")

#Converting to CGS
a = a[::-1]*M_Sun # reverse
b = np.power(10, b)
b = b[::-1]*R_Sun
c = np.power(10, c)
c = c[::-1]
d = np.power(10, d)
d = d[::-1]
e = e[::-1]
f = f[::-1]
g = g[::-1]

#The Cutout for wind/CSM
#wind_R_max = 1700*R_Sun # in cm together with progenitor
wind_R_max = (b[-1])+2250*R_Sun #only from progenitor
#wind_R_max = 1e15 # in cm

wind_Teff = 3500 #Kelvin
wind_Mdot = 1e-3*M_Sun/(365*24*3600) # in CGS
v0 = e[-1]
#v0 = 1e4
vinf = 1e6 # 10km/s in CGS
R0 = b[-1]
beta = 3

if wind_num != 0:
    delta_R_wind = (wind_R_max-R0)/wind_num
else:
    delta_R_wind = 0
#Function for beta law, mass and radius
def velobeta(v0, vinf, R0, r, beta):
    return v0 + (vinf-v0)*(1-(R0/r))**beta
def roCSM(v0, vinf, R0, r, beta, wind_Mdot):
    return wind_Mdot/(4*np.pi*velobeta(v0, vinf, R0, r, \
```

```
                                        beta))*r**(-2)
def diffofmass(v0, vinf, R0, r_1, r, beta, wind_Mdot):
        return (4*np.pi*(r**2)*(roCSM(v0, vinf, R0, r, \
            beta, wind_Mdot)+roCSM(v0, vinf, R0, r_1, beta, \
                           wind_Mdot))/2*delta_R_wind)

#Creating array for writing
Mass_Wind = 0
m = []
r = []
ro = []
ve = []
for j in range(wind_num):
    if j == 0:
                m.append(a[-1] + diffofmass(v0, vinf, R0, b[-1]+ \
                 (j)*delta_R_wind, \
                 b[-1]+(j+1)*delta_R_wind, beta, wind_Mdot))
        Mass_Wind += diffofmass(v0, vinf, R0, b[-1]+(j)*\
                                delta_R_wind, \
                                b[-1]+(j+1)*delta_R_wind, \
                                beta, wind_Mdot)

    else:
        m.append(m[-1] + diffofmass(v0, vinf, R0, b[-1]+(j)*\
                 delta_R_wind, b[-1]+(j+1)*delta_R_wind, beta,\
                 wind_Mdot))
        Mass_Wind += diffofmass(v0, vinf, R0, b[-1]+(j)*\
                                delta_R_wind, b[-1]+(j+1)*\
                                delta_R_wind, beta, wind_Mdot)
        r.append(b[-1]+(j+1)*delta_R_wind)
    ro.append(roCSM(v0, vinf, R0, b[-1]+ (j+1)*delta_R_wind,\
                    beta, wind_Mdot))
    ve.append(velobeta(v0, vinf, R0, b[-1]+(j+1)*delta_R_wind,\
                       beta))

#Writing between files profile -> short
for i in range(num):
    p_S.write("%d\t%.9E\t%.9E\t%.9E\t%.9E\t%.9E\t%.9E\t%.9E\n"\
              % (i+1, a[i], b[i], c[i], d[i], e[i], f[i], g[i]))
for i in range(wind_num):
    p_S.write("%d\t%.9E\t%.9E\t%.9E\t%.9E\t%.9E\t%.9E\t%.9E\n"\
              % (i+num+1, m[i], r[i], c[-1], ro[i], ve[i],\
                 f[-1], g[-1]))
#Closing the file
p_S.close()
```

```
isotopes = 15
iso = np.zeros((num, isotopes))
iso[::-1, 0] = f_M.data("neut") # neutron
iso[::-1, 1] = f_M.data("h1") + f_M.data("prot") # h1
iso[::-1, 2] = f_M.data("he4") + f_M.data("he3")# he4
iso[::-1, 3] = f_M.data("c12") + f_M.data("n14") # C12
iso[::-1, 4] = f_M.data("o16")
iso[::-1, 5] = f_M.data("ne20")
iso[::-1, 6] = f_M.data("mg24")
iso[::-1, 7] = f_M.data("si28")
iso[::-1, 8] = f_M.data("s32")
iso[::-1, 9] = f_M.data("ar36")
iso[::-1, 10] = f_M.data("ca40")
iso[::-1, 11] = f_M.data("ti44")
iso[::-1, 12] = f_M.data("cr48") + f_M.data("cr60") +\
 f_M.data("fe56")
iso[::-1, 13] = f_M.data("fe52") + f_M.data("fe54")
iso[::-1, 14] = f_M.data("ni56") + f_M.data("co56")

Ni = 0
#Converting final_model into iso.dat
f_S.write("%d\t%d\n" % (num+wind_num, isotopes))
f_S.write("1.0d0 1.0d0 4.0d0 12.0d0 16.0d0 20.0d0 24.0d0 \
          28.0d0 32.0d0 36.0d0 40.0d0 44.0d0 48.0d0 52.0d0 \
          56.0d0\n")
f_S.write("0.0d0 1.0d0 2.0d0 6.0d0 8.0d0 10.0d0 12.0d0 \
          14.0d0 16.0d0 18.0d0 20.0d0 22.0d0 24.0d0 26.0d0 \
          28.0d0\n")
for i in range(num):
    f_S.write("%.6E\t%.6E" % (a[i], b[i]))
    for j in range(isotopes):
        f_S.write("\t%.6E" % iso[i, j])
        if j==14:
            if i==1:
                Ni += iso[i, j]*a[i]
            else:
                Ni += iso[i, j]*(a[i]-a[i-1])
    f_S.write("\n")
    if i%100 == 0:
        total_mass = 0
        for k in range(isotopes):
            total_mass += iso[i, k]
        print("V kroku %d je total mass = %E percent \
              (malo by byť 100)" % (i, total_mass*100))
```

```
for i in range(wind_num):
    f_S.write("%.6E\t%.6E" % (m[i], r[i]))
    for j in range(isotopes):
        f_S.write("\t%.6E" % iso[-1, j])
    f_S.write("\n")
#Closing
print("Množstvo Ni v * = %E M_Sun" % (Ni/M_Sun))
f_S.close()

mass_to_sun = Mass_Wind/M_Sun
print("Hmotnosť windu = %E" % mass_to_sun)

print(b[-1]/R_Sun)
print(r[-1]/R_Sun)
```

Bibliography

[1] APPOURCHAUX, T., K. BELKACEM, A.-M. BROOMHALL, et al. *The Astronomy and Astrophysics Review* [online]. 2010, 18(1-2) [cit. 2019-05-15]. DOI: 10.1007/s00159-009-0027-z. ISSN 0935-4956. Avalaible from: http://link.springer.com/10.1007/s00159-009-0027-z

[2] BAADE, W., William P. CLASPY and John C. MARTIN. B Cassiopeiae as a Supernova of Type I. *The Astrophysical Journal* [online]. 1945, 102(761), 871-880 [cit. 2019-05-07]. DOI: 10.1086/144761. ISSN 0004-637X. Avalaible from: http://adsabs.harvard.edu/doi/10.1086/144761

[3] BENETTI, S., E. CAPPELLARO, M. TURATTO, S. TAUBENBERGER, A. HARUTYUNYAN a S. VALENTI. Supernova 2002ic: The Collapse of a Stripped-Envelope, Massive Star in a Dense Medium?. *The Astrophysical Journal* [online]. 2006, 653(2), L129-L132 [cit. 2019-05-08]. DOI: 10.1086/510667. ISSN 0004-637X. Avalaible from: http://stacks.iop.org/1538-4357/653/i=2/a=L129

[4] BOIAN, I. and J. H. GROH. *Catching a star before explosion: the luminous blue variable progenitor of SN 2015bh*. 2018, 617. DOI: 10.1051/0004-6361/201731794. ISSN 0004-6361. Avalaible from: https://www.aanda.org/10.1051/0004-6361/201731794

[5] BROWN, Peter J., Alice A. BREEVELD, Stephen HOLLAND, Paul KUIN and Tyler PRITCHARD. SOUSA: the Swift Optical/Ultraviolet Supernova Archive. *Astrophysics and Space Science* [online]. 2014, 354(1), 89-96 [cit. 2019-05-12]. DOI: 10.1007/s10509-014-2059-8. ISSN 0004-640X. Avalaible from: http://link.springer.com/10.1007/s10509-014-2059-8

[6] BRANCH, David, David J. JEFFERY, Jerod PARRENT, et al. Comparative Direct Analysis of Type Ia Supernova Spectra. IV. Postmaximum. *Publications of the Astronomical Society of the Pacific* [online]. 2008, 120(864), 135-149 [cit. 2019-05-13]. DOI: 10.1086/527572. ISSN 0004-6280. Avalaible from: http://iopscience.iop.org/article/10.1086/527572

[7] CATCHPOLE, R. M., J. W. MENZIES, A. S. MONK, et al. Spectroscopic and photometric observations of SN 1987a-II. Days 51 to 134. *Monthly Notices of the Royal Astronomical Society* [online]. 1987, 229(1), 15P-25P [cit. 2019-05-07]. DOI: 10.1093/mnras/229.1.15P. ISSN 0035-8711. Avalaible from: https://academic.oup.com/mnras/article-lookup/doi/10.1093/mnras/229.1.15P

[8] CHAKRABORTI, Sayan, Alak RAY, Randall SMITH, et al. PROBING FINAL STAGES OF STELLAR EVOLUTION WITH X-RAY OBSERVATIONS OF SN 2013ej. *The Astrophysical Journal* [online]. 2016, 817(1) [cit. 2019-05-12]. DOI: 10.3847/0004-637X/817/1/22. ISSN 1538-4357. Avalaible from: http://stacks.iop.org/0004-637X/817/i=1/a=22?key=crossref.0e5f70944624c79773c3e0a5064ce683

[9] CHEVALIER, R. A. Self-similar solutions for the interaction of stellar ejecta with an external medium. *The Astrophysical Journal* [online]. 1982, 258 [cit. 2019-05-07]. DOI: 10.1086/160126. ISSN 0004-637X. Avalaible from: http://adsabs.harvard.edu/doi/10.1086/160126

[10] CHEVALIER, Roger A. and Christopher M. IRWIN. SHOCK BREAKOUT IN DENSE MASS LOSS: LUMINOUS SUPERNOVAE. The Astrophysical Journal [online]. 2011, 729(1) [cit. 2019-05-08]. DOI: 10.1088/2041-8205/729/1/L6. ISSN 2041-8205. Avalaible from: http://stacks.iop.org/2041-8205/729/i=1/a=L6?key=crossref.8756ced077e9151037772d5dc3b83f11

[11] CHUGAI, N. N. SN 2011ht: A weak explosion in a massive extended envelope. *Astronomy Letters* [online]. 2016, 42(2), 82-89 [cit. 2019-05-02]. DOI: 10.1134/S106377371602002X. ISSN 1063-7737. Avalaible from: http://link.springer.com/10.1134/S106377371602002X

[12] COLLINS II, George W., William P. CLASPY and John C. MARTIN. A Reinterpretation of Historical References to the Supernova of a.d. 1054. *Publications of the Astronomical Society of the Pacific* [online]. 1999, 111(761), 871-880 [cit. 2019-05-07]. DOI: 10.1086/316401. ISSN 0004-6280. Avalaible from: http://iopscience.iop.org/article/10.1086/316401

[13] DONG, S., B. J. SHAPPEE, J. L. PRIETO, et al. ASASSN-15lh: A highly super-luminous supernova. *Science* [online]. 2016, 351(6270), 257-260 [cit. 2019-05-03]. DOI: 10.1126/science.aac9613. ISSN 0036-8075. Avalaible from: http://www.sciencemag.org/cgi/doi/10.1126/science.aac9613

[14] DWARKADAS, V. V. On luminous blue variables as the progenitors of core-collapse supernovae, especially Type IIn supernovae. *Monthly Notices of the Royal Astronomical Society* [online]. 2011, 412(3), 1639-1649 [cit. 2019-05-07]. DOI: 10.1111/j.1365-2966.2010.18001.x. ISSN 00358711. Avalaible from: https://academic.oup.com/mnras/article-lookup/doi/10.1111/j.1365-2966.2010.18001.x

[15] FARMER, R., C. E. FIELDS, I. PETERMANN, Luc DESSART, M. CANTIELLO, B. PAXTON and F. X. TIMMES. ON VARIATIONS OF PRE-SUPERNOVA MODEL PROPERTIES. *The Astrophysical Journal Supplement Series* [online]. 2016, 227(2) [cit. 2019-05-01]. DOI: 10.3847/1538-4365/227/2/22. ISSN 1538-4365. Avalaible from: http://stacks.iop.org/0067-0049/227/i=2/a=22?key=crossref.eab082d2cd46050689c7a820bc17cce9

[16] FRIEMAN, Joshua A., Michael S. TURNER and Dragan HUTERER. Dark Energy and the Accelerating Universe. *Annual Review of Astronomy and Astrophysics* [online]. 2008, 46(1), 385-432 [cit. 2019-05-14]. DOI: 10.1146/annurev.astro.46.060407.145243. ISSN 0066-4146. Avalaible from: http://www.annualreviews.org/doi/10.1146/annurev.astro.46.060407.145243

[17] GARCIA-BELLIDO, Juan. *Modern cosmology: 32nd International Meeting on Fundamental Physics (IMFP2004) Alicante* , Spain, March 1-5, 2004 [online]. 2004 [cit. 2019-05-6]. Avalaible from: https://arxiv.org/abs/hep-ph/0407111

[18] GUILLOCHON, James, Jerod PARRENT, Luke Zoltan KELLEY and Raffaella MARGUTTI. An Open Catalog for Supernova Data. The Astrophysical Journal [online]. 2017, 835(1) [cit. 2019-05-2]. DOI: 10.3847/1538-4357/835/1/64. ISSN 1538-4357. Avalaible from: http://stacks.iop.org/0004-637X/835/i=1/a=64?key=crossref.10c8a4c42be03c3ea345fd583d5b930a

[19] GUTIÉRREZ, Claudia P., Joseph P. ANDERSON, Mario HAMUY, et al. Type II Supernova Spectral Diversity. I. Observations, Sample Characterization, and Spectral Line Evolution. *The Astrophysical Journal* [online]. 2017, 850(1) [cit. 2019-05-3]. DOI: 10.3847/1538-4357/aa8f52. ISSN 1538-4357. Avalaible from: http://stacks.iop.org/0004-637X/850/i=1/a=89?key=crossref.eb747803b78b3fcfd805d066aba99253

[20] HANKE, Florian, Bernhard MÜLLER, Annop WONGWATHANARAT, Andreas MAREK a Hans-Thomas JANKA. SASI ACTIVITY IN THREE-DIMENSIONAL NEUTRINO-HYDRODYNAMICS SIMULATIONS OF SUPERNOVA CORES. *The Astrophysical Journal* [online]. 2013, 770(1) [cit. 2019-05-6]. DOI: 10.1088/0004-637X/770/1/66. ISSN 0004-637X. Avalaible from: http://stacks.iop.org/0004-637X/770/i=1/a=66?key=crossref.67519a09268b611679c1e27dd77fcdab

[21] HARMANEC, Petr.*Stavba a vývoj hvězd* [online]. Verze 7. Praha: Matfyzpress, 2008 [cit. 2019-05-07]. Avalaible from: http://astro.mff.cuni.cz/hec/AST014/ast014.pdf

[22] HUANG, Fang, Xiaofeng WANG, Jujia ZHANG, et al. SN 2013ej IN M74: A LUMINOUS AND FAST-DECLINING TYPE II-P SUPERNOVA. *The Astrophysical Journal* [online]. 2015, 807(1) [cit. 2019-05-12]. DOI: 10.1088/0004-637X/807/1/59. ISSN 1538-4357. Avalaible from: http://stacks.iop.org/0004-637X/807/i=1/a=59?key=crossref.c12f227c38a916e591c33c008985bc3f

[23] JANKA, Hans-Thomas. Neutrino Emission from Supernovae. *Handbook of Supernovae* [online]. Cham: Springer International Publishing, 2017, 2017-11-15, , 1575-1604 [cit. 2019-05-13]. DOI: 10.1007/978-3-319-21846-5_4. ISBN 978-3-319-21845-8. Avalaible from: http://link.springer.com/10.1007/978-3-319-21846-5_4

[24] JANKA, H, K LANGANKE, A MAREK, G MARTINEZPINEDO and B MULLER. Theory of core-collapse supernovae. *Physics Reports* [online]. 2007, 442(1-6), 38-74 [cit. 2019-05-07]. DOI: 10.1016/j.physrep.2007.02.002. ISSN 03701573. Avalaible from: https://linkinghub.elsevier.com/retrieve/pii/S0370157307000439

[25] KASEN, Daniel a S. E. WOOSLEY. TYPE II SUPERNOVAE: MODEL LIGHT CURVES AND STANDARD CANDLE RELATIONSHIPS. *The Astrophysical Journal* [online]. 2009, 703(2), 2205-2216 [cit. 2019-05-10]. DOI: 10.1088/0004-637X/703/2/2205. ISSN 0004-637X. Avalaible from: http://stacks.iop.org/0004-637X/703/i=2/a=2205?key=crossref.208d40b300652b1e492e00d8bcc4f81f

[26] Kepler's Supernova Remnant in X-Rays. In: *Astronomy Picture of the Day* [online]. NASA, 2015 [cit. 2019-05-16]. Dostupné z: https://apod.nasa.gov/apod/image/1305/keplersnr_chandra_3600.jpg

[27] LEBLANC, Francis. *An introduction to stellar astrophysics.* Chichester, West Sussex, U.K.: Wiley, 2010. ISBN 0470699566.

[28] LÉPINE-SZILY, Alinka a Pierre DESCOUVEMONT. Nuclear astrophysics: nucleosynthesis in the Universe. *International Journal of Astrobiology* [online]. 2012, 11(4), 243-250 [cit. 2019-05-16]. DOI: 10.1017/S1473550412000158. ISSN 1473-5504. Avalaible from: https://www.cambridge.org/core/product/identifier/S1473550412000158/type/journal_article

[29] LONGAIR, Malcolm S. *High energy astrophysics*. 3rd ed. New York: Cambridge University Press, 2011. ISBN 978-0-521-75618-1.

[30] MA, H., S. E. WOOSLEY, C. M. MALONE, A. ALMGREN a J. BELL. CARBON DEFLAGRATION IN TYPE Ia SUPERNOVA. I. CENTRALLY IGNITED MODELS. *The Astrophysical Journal* [online]. 2013, 771(1) [cit. 2019-05-07]. DOI: 10.1088/0004-637X/771/1/58. ISSN 0004-637X. Available from: http://stacks.iop.org/0004-637X/771/i=1/a=58?key=crossref.897d9c4dcd7c214e49d091d2ec5916e0

[31] MAEDER, André. *Physics, formation and evolution of rotating stars.* London: Springer, c2009. Astronomy and astrophysics library. ISBN 978-3-540-76948-4.

[32] MAUERHAN, Jon C., Nathan SMITH, Jeffrey M. SILVERMAN, et al. SN 2011ht: confirming a class of interacting supernovae with plateau light curves (Type IIn-P). *Monthly Notices of the Royal Astronomical Society* [online]. 2013, 431(3), 2599-2611 [cit. 2019-05-12]. DOI: 10.1093/mnras/stt360. ISSN 1365-2966. Avalaible from: http://academic.oup.com/mnras/article/431/3/2599/1077931/SN-2011ht-confirming-a-class-of-interacting

[33] MORIYA, Takashi. *Supernovae Interacting with Circumstellar Media*. 2013. Phd Thesis. University of Tokyo, Department of Astronomy, Graduate School of Science.

[34] MORIYA, Takashi, Nozomu TOMINAGA, Sergei I. BLINNIKOV, Petr V. BAKLANOV and Elena I. SOROKINA. Supernovae from red supergiants with extensive mass loss. *Monthly Notices of the Royal Astronomical Society* [online]. 2011, 415(1), 199-213 [cit. 2019-05-12]. DOI: 10.1111/j.1365-2966.2011.18689.x. ISSN 00358711. Avalaible from: https://academic.oup.com/mnras/article-lookup/doi/10.1111/j.1365-2966.2011.18689.x

[35] MOROZOVA, Viktoriya, Anthony L. PIRO, Mathieu RENZO, Christian D. OTT, Drew CLAUSEN, Sean M. COUCH, Justin ELLIS and Luke F. ROBERTS. LIGHT CURVES OF CORE-COLLAPSE SUPERNOVAE WITH SUBSTANTIAL MASS LOSS USING THE NEW OPEN-SOURCE SUPERNOVA EXPLOSION CODE (SNEC). *The Astrophysical Journal* [online]. 2015, 814(1) [cit. 2019-05-07]. DOI: 10.1088/0004-637X/814/1/63. ISSN 1538-4357. Avalaible from: http://stacks.iop.org/0004-637X/814/i=1/a=63?key=crossref.5c1e9f7612a2d7e4ca6beb41549183f8 The code is avalaible from: http://stellarcollapse.org/SNEC.

[36] MOROZOVA, Viktoriya, Anthony L. PIRO and Stefano VALENTI. Unifying Type II Supernova Light Curves with Dense Circumstellar Material. *The Astrophysical Journal* [online]. 2017, 838(1) [cit. 2019-05-09]. DOI: 10.3847/1538-4357/aa6251. ISSN 1538-4357. Avalaible from: http://stacks.iop.org/0004-637X/838/i=1/a=28?key=crossref.e2c25dab763b5fa9d01d3509be0f449f

[37] LC of Type II-L vs II-P. In: COSMOS - The SAO Encyclopedia of Astronomy [online]. Hawthorn: Swinburne University of Technology, 2015 [cit. 2019-05-16]. Avalaiable from: http://astronomy.swin.edu.au/cms/cpg15x/albums/userpics/typeiilightcurves1.gif

[38] MATZNER, Christopher D. a Christopher F. MCKEE. The Expulsion of Stellar Envelopes in Core-Collapse Supernovae. *The Astrophysical Journal* [online]. 1999, 510(1), 379-403 [cit. 2019-05-05]. DOI: 10.1086/306571. ISSN 0004-637X. Avalaible from: http://stacks.iop.org/0004-637X/510/i=1/a=379

[39] OSTLIE, Dale A. a Bradley W. CARROLL. *An introduction to modern stellar astrophysics*. Reading, Mass.: Addison-Wesley Pub., c1996. ISBN 0201598809.

[40] PAXTON, Bill, Lars BILDSTEN, Aaron DOTTER, Falk HERWIG, Pierre LESAFFRE and Frank TIMMES. MODULES FOR EXPERIMENTS IN STELLAR ASTROPHYSICS (MESA). *The Astrophysical Journal Supplement Series* [online]. 2011, 192(1) [cit. 2019-05-07]. DOI: 10.1088/0067-0049/192/1/3. ISSN 0067-0049. Avalaible from: http://stacks.iop.org/0067-0049/192/i=1/a=3?key=crossref.4bfe81c8d21794a47ae04409880eee28

[41] PAXTON, Bill, Matteo CANTIELLO, Phil ARRAS, et al. MODULES FOR EXPERIMENTS IN STELLAR ASTROPHYSICS (MESA): PLANETS, OSCILLATIONS, ROTATION, AND MASSIVE STARS. *The Astrophysical Journal Supplement Series* [online]. 2013, 208(1) [cit. 2019-05-07]. DOI: 10.1088/0067-0049/208/1/4. ISSN 0067-0049. Avalaible from: http://stacks.iop.org/0067-0049/208/i=1/a=4?key=crossref.9ac89c257bf3021e94c56104e0913fc9

[42] ROGERS, F. J. a A. NAYFONOV. Updated and Expanded OPAL Equation-of-State Tables: Implications for Helioseismology. *The Astrophysical Journal* [online]. 2002, 576(2), 1064-1074 [cit. 2019-05-04]. DOI: 10.1086/341894. ISSN 0004-637X. Avalaible from: http://stacks.iop.org/0004-637X/576/i=2/a=1064

[43] ROSSWOG, Stephan and Marcus BRÜGGEN. *Introduction to high-energy astrophysics.* New York: Cambridge University Press, 2007. ISBN 0521857694

[44] RUBIN, Adam, Avishay GAL-YAM, Annalisa DE CIA, et al. TYPE II SUPERNOVA ENERGETICS AND COMPARISON OF LIGHT CURVES TO SHOCK-COOLING MODELS. *The Astrophysical Journal* [online]. 2016, 820(1) [cit. 2019-05-02]. DOI: 10.3847/0004-637X/820/1/33. ISSN 1538-4357. Avalaible from: http://stacks.iop.org/0004-637X/820/i=1/a=33?key=crossref.05551e8281e4458cab30d5c7e4fc671f

[45] SCHLEGEL, Eric. A new subclass ofType II Supernovae?. Monthly Notices of the Royal Astronomical Society [online]. 1990, 1990(vol. 244), 269-271 [cit. 2019-05-08]. ISSN 0035-8711. Avalaible from: http://adsabs.harvard.edu/abs/1990MNRAS.244..269S

[46] SHU, Frank H. *The physics of astrophysics*. Mill Valley, Calif.: University Science Books, c1991. ISBN 09-357-0265-2.

[47] SMITH, Nathan. Interacting Supernovae: Types IIn and Ibn. *Handbook of Supernovae* [online]. Cham: Springer International Publishing, 2017, 2017-11-15, , 403-429 [cit. 2019-05-07]. DOI: 10.1007/978-3-319-21846-5_38. ISBN 978-3-319-21845-8. Avalaible from: http://link.springer.com/10.1007/978-3-319-21846-5_38

[48] SNIacurva. In: Wikipedia [online]. San Francisco: Wikimedia Foundation, 2005 [cit. 2019-05-16]. Avalaible from: https://en.wikipedia.org/wiki/Type_Ia_supernova#/media/File:SNIacurva.png

[49] SORLIN, O. a M.-G. PORQUET. Nuclear magic numbers: New features far from stability. *Progress in Particle and Nuclear Physics* [online]. 2008, 61(2), 602-673 [cit. 2019-04-08]. DOI: 10.1016/j.ppnp.2008.05.001. ISSN 01466410. Avalaible from: https://linkinghub.elsevier.com/retrieve/pii/S0146641008000380

[50] SUKHBOLD, Tuguldur and S. E. WOOSLEY. THE MOST LUMINOUS SUPERNOVAE. *The Astrophysical Journal* [online]. 2016, 820(2) [cit. 2019-05-12]. DOI: 10.3847/2041-8205/820/2/L38. ISSN 2041-8213. Avalaible from: http://stacks.iop.org/2041-8205/820/i=2/a=L38?key=crossref.42827d4c8441c5e4034a5e93cc511965

[51] SUPERNOVA 1987A IN THE LARGE MAGELLANIC CLOUD. Central Bureau for Astronomical Telegrams [online]. [cit. 2019-03-10]. Avalaible from: http://www.cbat.eps.harvard.edu/iauc/04300/04316.html

[52] SUPERNOVA 1999aa IN NGC 2595. Central Bureau for Astronomical Telegrams [online]. [cit. 2019-03-10]. Avalaible from: http://www.cbat.eps.harvard.edu/iauc/07100/07109.html

[53] ŠTEFL, Vladimír a Jiří KRTIČKA. *HISTORIE ASTRONOMIE* [online]. Brno, 2008 [cit. 2019-05-07]. Avalaible from: http://www.physics.muni.cz/astrohistorie/historie.pdf

[54] TORNAMBÉ, A. a L. PIERSANTI. Pre-explosive observational properties of Type Ia supernovae. *Monthly Notices of the Royal Astronomical Society* [online]. 2013, 431(2), 1812-1822 [cit. 2019-05-14]. DOI: 10.1093/mnras/stt295. ISSN 1365-2966. Avalaible from: http://academic.oup.com/mnras/article/431/2/1812/1465884/Preexplosive-observational-properties-of-TypeIa

[55] VALENTI, S., D. A. HOWELL, M. D. STRITZINGER, et al. The diversity of Type II supernova versus the similarity in their progenitors. *Monthly Notices of the Royal Astronomical Society* [online]. 2016, 459(4), 3939-3962 [cit. 2019-05-12]. DOI: 10.1093/mnras/stw870. ISSN 0035-8711. Avalaible from: https://academic.oup.com/mnras/article-lookup/doi/10.1093/mnras/stw870

[56] VANÝSEK, Vladimír. *Základy astronomie a astrofyziky.* Praha: Academie, 1980.

[57] VINK, Jacco. Supernova 1604, Kepler's Supernova, and its Remnant. *Handbook of Supernovae* [online]. Cham: Springer International Publishing, 2017, 2017-11-15, , 139-160 [cit. 2019-05-07]. DOI: 10.1007/978-3-319-21846-5_49. ISBN 978-3-319-21845-8. Avalaible from: http://link.springer.com/10.1007/978-3-319-21846-5_49

[58] WERNER, Norbert. Own notes from the lecture, course: *High Energy Astrophysics*, autumn 2018.

[59] WINKLER, P. Frank, Gaurav GUPTA and Knox S. LONG. The SN 1006 Remnant: Optical Proper Motions, Deep Imaging, Distance, and Brightness at Maximum. *The Astrophysical Journal* [online]. 2003, 585(1), 324-335 [cit. 2019-04-07]. DOI: 10.1086/345985. ISSN 0004-637X. Avalaible from: http://stacks.iop.org/0004-637X/585/i=1/a=324

[60] YUAN, Fang, A. JERKSTRAND, S. VALENTI, et al. *Monthly Notices of the Royal Astronomical Society* [online]. 2016, 461(2) [cit. 2019-05-12]. DOI: 10.1093/mnras/stw1419. ISSN 0035-8711. Avalaible from: https://academic.oup.com/mnras/article-lookup/doi/10.1093/mnras/stw1419